CONTENT
Vol. 7. No. 6-2021

Published bi-monthly since 2015.

ISSN 2664-066X (Print)
ISSN 2664-0678 (Online)

Publisher
Institute of Radio and Information Systems (IRIS), Vienna, Austria

Address:
1010 Wien, Austria,
Ebendorferstrasse 10/6b
media-publisher.eu/
synchroinfo-journal

NONLINEAR DISTORTION AND NOISE ANALYSIS OF GENERAL G_M-C FILTERS

S. Koziel, S. Szczepanski,
Faculty of Electronics, Telecommunications and Inf., Gdansk University of Technology, Gdansk, Poland

E. Sanchez-Sinencio,
Department of Electrical Engineering Texas A&M University, College Station, USA

DOI: 10.36724/2664-066X-2021-7-6-2-7

ABSTRACT

Systems such as G_m-C filters are ideally designed to exhibit linear characteristics. However, their components – especially transconductors – are intrinsically nonlinear. Although there exist many approaches that aim at reducing nonlinear effects while dealing with practical design problems, nonlinear distortion cannot be canceled out completely. Thus, it is important to estimate a degradation of filter performance caused by nonlinearities. In this paper we propose a simple and general method to perform a transient analysis of any G_m-C filter structure based on a matrix description and macromodeling of transconductors. An analytical description of general G_m-C filters with nonlinear transconductors is introduced. A differential system that determines dynamics of a general structure of G_m-C filter is formulated. This allows us to carry out an effective and fast transient analysis of any G_m-C filter using standard numerical methods. The approach can be applied to investigate any nonlinear effects in filters. The noise analysis of G_m-C filters in general setting is also presented. The accuracy of the proposed methods is confirmed by comparison with SPICE simulation. Example of application for performance optimization of 4th order Chebyshev filter is given.

KEYWORDS: *G_m-C filters, nonlinear effects, noise analysis.*

The article is reworked from unpublished 2nd IEEE International Conference on Circuits and Systems for Communications (ICCSC) materials.

Introduction

There has been a growing interest displayed in the design of continuous-time (CT) filters based on the transconductance-capacitor (G_m-C) technique for more than two decades [1], [2].

The operational transconductance amplifiers (OTAs) offer a higher bandwidth than their voltage-mode counterparts, can be easily tuned electronically, and have a better suitability for operating in reduced supply environment [3]-[5]. Due to this, high frequency integrated filters are mostly realized as the G_m-C ones [6].

Systems such as G_m-C filters are ideally designed to exhibit linear characteristics. However, their components - especially transconductors – are intrinsically nonlinear. Although there exist many approaches that aim at reducing nonlinear effects while dealing with practical design problems (see e.g. tutorial paper [7]), nonlinear distortion cannot be canceled out completely.

Thus, it is important to estimate a degradation of filter performance caused by nonlinearities. In this paper we propose a simple and general method to perform a transient analysis of any G_m-C filter structure based on a matrix description and macromodeling of transconductors.

Thisis a very fast and efficient procedure. Unlike the approaches based on Volterra series representation [8],[9] or harmonic injection method [10], it is not restricted to handle weak nonlinearities only. The noise analysis of general G_m-C filter is also included, which allows us to calculate Dynamic Range (DR) for arbitrary G_m-C filter.

Dynamics of nonlinear G_M-C filters

Consider a general structure of G_m-C filter shown in Figure 1. The structure in Fig.1 contains n internal nodes denoted as x_i, i=1,...,n, n input transconductors G_{bi}, the set of internal feedback and feedforward transconductors G_{mij}, an output summer consisting of transconductors G_{ci} and G_o as well as a feedforward transconductor G_d.

We assume that in general transconductors are not linear. All transconductors form *active network*, while input capacitors C_{bi}, i=1,...,n and capacitors C_{ij}, 1_i<j_n form *passive network*. It is easily seen that any G_m-C filter is a particular case of the general structure in Figure1.

We shall derive an analytical description of the considered structure in the time domain. In the following considerations we will denote the voltage at the i-th node x_i also by x_i, which will not lead to confusion. Symbols u_i, u_o will denote the input and output voltages, respectively. The rest of the necessary notation is introduced in Figure 2.

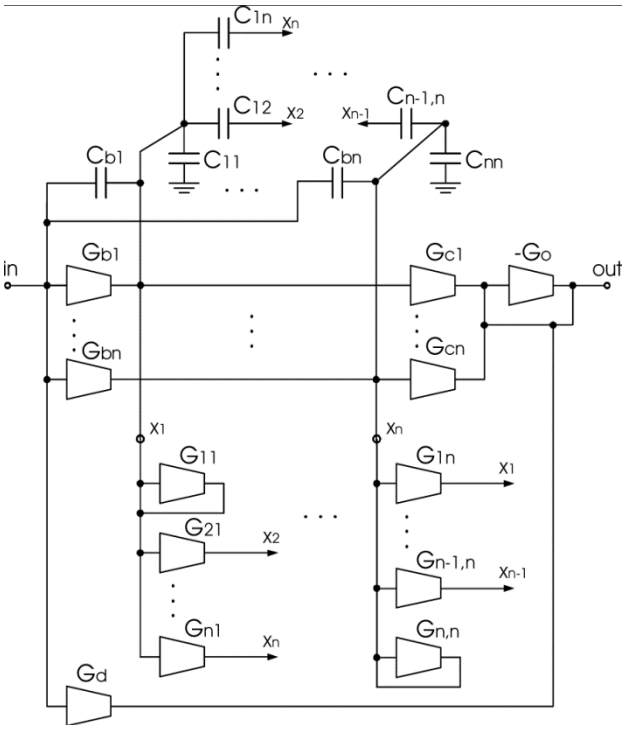

Fig. 1. General structure of Gm-C filter

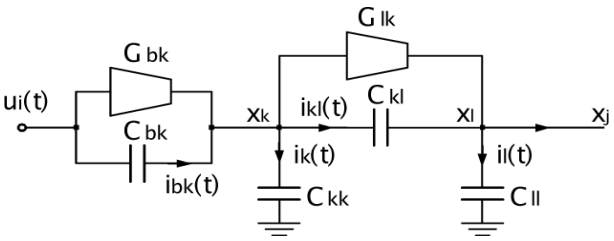

Fig. 2. Part of the circuit in Figure1 with the notation used to its analytical description

According to the notation introduced in Figure 2, the general structure of G_m-C filter in Figure 1 can be described by the following system of integral equations:

$$x_k(t) = \frac{1}{C_{kk}} \int_0 i_k(s)ds + x_k(0), \quad (1)$$

$$x_k(t) - x_l(t) = \frac{1}{C_{kl}} \int_0 i_{kl}(s)ds + x_k(0) - x_l(0), \quad (k<l) \quad (2)$$

$$u_i(t) - x_k(t) = \frac{1}{C_{bk}} \int_0 i_{bk}(s)ds + u_i(0) - x_k(0), \quad (3)$$

$$-\sum_{q=1,\, q\neq k}^{n} i_{qk}(t) + i_k(t) - i_{bk}(t) = \sum_{q=1}^{n} G_{kq}\left(x_q(t)\right) + G_{bk}\left(u_i(t)\right), \quad (4)$$

$$u_o(t) = -G_o^{-1}\left(\sum_{l=1}^{n} G_{cl}\left(x_l(t)\right) + G_d\left(u_i(t)\right)\right), \quad (5)$$

where $k,l=1,...,n$, $k<l$. Note that G_{kl}, G_{bk}, G_{cl}, G_d and G_o, $k,l=1,2,...,n$ are in general nonlinear functions of their input variables. Define vectors $\boldsymbol{x}(t)$ and $\boldsymbol{x}'(t)$ as

$$\boldsymbol{x}(t)=\begin{bmatrix}x_1(t) & \cdots & x_n(t)\end{bmatrix}^T,\quad \dot{\boldsymbol{x}}(t)=\begin{bmatrix}\dot{x}_1(t) & \cdots & \dot{x}_n(t)\end{bmatrix}^T, \qquad (6)$$

and matrix $\boldsymbol{T}_C$ as

$$\boldsymbol{T}_C=\begin{bmatrix} C_{b1}+\sum_{j=1}^{n}C_{1j} & -C_{12} & \cdots & -C_{1n} \\ -C_{12} & C_{b2}+\sum_{j=1}^{n}C_{2j} & \cdots & -C_{2n} \\ \vdots & \vdots & \ddots & \vdots \\ -C_{1n} & -C_{2n} & \cdots & C_{bn}+\sum_{j=1}^{n}C_{nj} \end{bmatrix}. \qquad (7)$$

Using (6) and (7), the system (1)-(4) can be rewritten in equivalent differential form as:

$$\boldsymbol{T}_C\,\dot{\boldsymbol{x}}(t)=\begin{bmatrix}\sum_{l=1}^{n}G_{1l}(x_l(t))\\ \vdots \\ \sum_{l=1}^{n}G_{nl}(x_l(t))\end{bmatrix}+\begin{bmatrix}G_{b1}(u_i(t))+C_{b1}\dot{u}_i(t)\\ \vdots \\ G_{bn}(u_i(t))+C_{bn}\dot{u}_i(t)\end{bmatrix}, \qquad (8)$$

Let us now consider a special case, where all transconductors are linear, i.e. we have $G_{kl}(y)=g_{kl}y$, $G_{bk}(y)=g_{bk}y$, $G_{cl}(y)=g_{cl}y$, $G_d(y)=g_dy$ and $G_o(y)=g_oy$, $k,l=1,2,...,n$. Define the following matrices:

$$\boldsymbol{G}=\begin{bmatrix} g_{11} & g_{12} & \cdots & g_{1n} \\ g_{21} & g_{22} & \cdots & g_{2n} \\ \vdots & \vdots & \ddots & \vdots \\ g_{n1} & g_{n2} & \cdots & g_{nn} \end{bmatrix},\quad \boldsymbol{C}=\begin{bmatrix}c_1 & \cdots & c_n\end{bmatrix}, \qquad (9)$$

$$\boldsymbol{B}=\begin{bmatrix} g_{b1}+C_{b1}\dfrac{d}{dt} & \cdots & g_{bn}+C_{bn}\dfrac{d}{dt}\end{bmatrix}^T,\quad \boldsymbol{D}=d, \qquad (10)$$

with $c_i=-g_{ci}/g_o$, $i=1,2,...,n$ and $d=-g_d/g_o$. Using this notation we can rewrite (8), (5) as follows:

$$\boldsymbol{T}_C\dot{\boldsymbol{x}}(t)=\boldsymbol{G}\boldsymbol{x}(t)+\boldsymbol{B}u_i(t),\qquad u_o(t)=\boldsymbol{C}\boldsymbol{x}(t)+\boldsymbol{D}u_i(t), \qquad (11)$$

or, in the domain of Laplace transform:

$$s\boldsymbol{T}_C\boldsymbol{X}=\boldsymbol{G}\boldsymbol{X}+\boldsymbol{B}u_i,\qquad u_o=\boldsymbol{C}\boldsymbol{X}+\boldsymbol{D}u_i, \qquad (12)$$

in which $\boldsymbol{X}$ is the Laplace transform of the vector $\boldsymbol{x}$.

System (12) is the state variable matrix description of the general structure of a voltage-mode Gm-C filter introduced in [11]. Thus, system (12) is a particular (linear) case of the general (nonlinear) system describing a filter circuit in Figure 1.

Let us turn back to the general case. If the matrix $\boldsymbol{T}_C$ is invertible, equation (8) can be reformulated as

$$\dot{\boldsymbol{x}}(t)=\boldsymbol{T}_C^{-1}\left(\begin{bmatrix}\sum_{l=1}^{n}G_{1l}(x_l(t))\\ \vdots \\ \sum_{l=1}^{n}G_{nl}(x_l(t))\end{bmatrix}+\begin{bmatrix}G_{b1}(u_i(t))+C_{b1}\dot{u}_i(t)\\ \vdots \\ G_{bn}(u_i(t))+C_{bn}\dot{u}_i(t)\end{bmatrix}\right). \qquad (13)$$

The above assumption is very natural. In particular, it is satisfied if every internal node of the filter has a grounded capacitor. The problem of invertibility of matrix $\boldsymbol{T}_C$ has been thoroughly addressed in [11].

Denote the vector on the right-hand side of (13) by $f(u(t), \boldsymbol{x}(t))$. Then we have

$$\dot{\boldsymbol{x}}(t)=f(u(t),\boldsymbol{x}(t)), \qquad (14)$$

By endowing (14) with an initial condition

$$\boldsymbol{x}(0)=(x_{0.1},...,x_{0.n}), \qquad (15)$$

we arrive at a classical Cauchy problem which can be easily solved numerically.

The above model can be applied to calculate THD of any Gm-C filter for given input voltage frequency and amplitude. It is enough to integrate system (14), (15) with natural initial condition $x_{0.k}=0$ for $k=1,2,...,n$ and calculate THD by definition, i.e.

$$THD=\sqrt{\sum_{n=2}^{\infty}C_n^2\Big/\sum_{n=1}^{\infty}C_n^2}\approx\sqrt{\sum_{n=2}^{N}C_n^2\Big/\sum_{n=1}^{N}C_n^2}, \qquad (16)$$

where

$$C_n=\frac{2}{T}\left|\int_{-T/2}^{T/2}u_0(t)e^{-j2n\pi t/T}dt\right|,\qquad n=1,2,... \qquad (17)$$

and N is integer chosen so as to make the approximation in (16) good enough (here $|z|$ denotes modulus of the complex number z). Obviously, coefficients C_n can be determined numerically using $u_0(t)$ obtained from (5).

Noise analysis

The output noise of any Gm-C filter is a combination of the noise contributions of its all transconductors. The noise in CMOS amplifier with transconductance g_m can be described in terms of an equivalent input referred noise voltage. Its spectral density $S_n(f)$ can be modeled as [12]:

$$S_n(f)=S_w/g_m+S_f/f \qquad (18)$$

where both S_w and S_f depend on amplifier topology. Since each transconductor injects its noise current (its spectrum density equals $S_ng_m^2$) into one of the internal nodes of the filter, its contribution to the output noise spectrum is determined by the current-to-voltage transfer function from the respective node to the output of the filter.

It can be shown using (12) that the current-to-voltage transfer function $H_i(s)$ from i-th node to the output of the filter is

$$H_i(s) = \left(\boldsymbol{C}(s\boldsymbol{T}_C - \boldsymbol{G})^{-1}\right)_i \tag{19}$$

i.e. H_i is the i-th component of vector $\boldsymbol{H}_{cv}(s) = \boldsymbol{C}(s\boldsymbol{T}_c - \boldsymbol{G})^{-1}$, where $\boldsymbol{T}_c$, $\boldsymbol{G}$ and $\boldsymbol{C}$ are given by (7) and (9), respectively. The elements of $\boldsymbol{G}$ and $\boldsymbol{C}$ are, in general, first order terms in the Taylor series expansion of the transconductor transfer functions. If non-trivial output summer is present (Fig. 1) then one has also take into consideration the noise of transconductors G_{ci}, G_d and G_o. The current-to-voltage transfer function from output node to itself is $H_0 = g_0^{-1}$. Define the matrices

$$\begin{aligned}
&\boldsymbol{S}_w = \left[S_{w.ij}\right]_{i,j=1}^n, && \boldsymbol{S}_f = \left[S_{f.ij}\right]_{i,j=1}^n \\
&\boldsymbol{S}_{wb} = \left[S_{wb.i}\right]_{i=1}^n, && \boldsymbol{S}_{fb} = \left[S_{fb.i}\right]_{i=1}^n \\
&\boldsymbol{S}_{wc} = \left[S_{wc.i}\right]_{i=1}^n, && \boldsymbol{S}_{fc} = \left[S_{fc.i}\right]_{i=1}^n \\
&\boldsymbol{S}_{wd} = S_{wd}, \quad \boldsymbol{S}_{fd} = S_{fd}, && \boldsymbol{S}_{wo} = S_{wo}, \quad \boldsymbol{S}_{fo} = S_{fo}
\end{aligned} \tag{20}$$

representing the white noise (subscript w) and $1/f$ noise (subscript f) of transconductors g_{ij}, g_{bi}, g_{ci}, g_d and g_o, respectively.

Let $\overline{\boldsymbol{G}} = [\,|g_{ij}|\,]_{i,j=1}^n$, $\overline{\boldsymbol{B}} = [\,|g_{bi}|\,]_{i=1}^n$, $\overline{\boldsymbol{C}} = [\,|g_{ci}|\,]_{i=1}^n$, $\overline{\boldsymbol{D}} = |g_d|$, $\overline{\boldsymbol{O}} = |g_o|$. Denote by the Hadamard product of two matrices, i.e. for $\boldsymbol{A} = [a_{ij}]_{i,j=1}^n$ and $\boldsymbol{B} = [b_{ij}]_{i,j=1}^n$ we have $\boldsymbol{A} \circ \boldsymbol{B} = [a_{ij}b_{ij}]_{i,j=1}^n$ (the same definition holds, with obvious changes for $n\times1$, $1\times n$ and 1×1 matrices). The output noise spectrum $u_{no}^2(\omega)$ of the filter can be then calculated as

$$\begin{aligned}
u_{no}^2(\omega) = |\boldsymbol{H}_{cv}(\omega)|^2 \left[P(\overline{\boldsymbol{G}}, \boldsymbol{S}_w, \boldsymbol{S}_f)(\omega)\cdot\hat{\boldsymbol{I}} + P(\overline{\boldsymbol{B}}, \boldsymbol{S}_{wb}, \boldsymbol{S}_{fb})(\omega)\right]^T + \\
+ H_0^2\left[P(\overline{\boldsymbol{C}}, \boldsymbol{S}_{wc}, \boldsymbol{S}_{fc})\cdot\hat{\boldsymbol{I}} + P(\overline{\boldsymbol{D}}, S_{wd}, S_{fd}) + P(\overline{\boldsymbol{O}}, S_{wo}, S_{fo})\right]
\end{aligned} \tag{21}$$

where $|\boldsymbol{H}_{cv}(\omega)|^2 = \boldsymbol{H}_{cv}(j\omega) \circ \boldsymbol{H}_{cv}(-j\omega)$ and the function P is defined as: $P(\boldsymbol{A}, \boldsymbol{B}, \boldsymbol{C})(\omega) = \boldsymbol{A} \circ (\boldsymbol{B} + (2\pi/\omega)\boldsymbol{A} \circ \boldsymbol{C})$, and $\hat{\boldsymbol{I}} = [1 \ \cdots \ 1]^T$ is $n\times1$ vector.

In general, $u^2_{no}(\omega)$ is a rational function of ω with numerator and denominator of order not larger than $2n$-1 and $2n$+1, respectively.

Formula (21) allows us to calculate the output noise spectrum of any Gm-C filter. In order to get the output noise voltage one needs to integrate (21) over the suitable frequency range. The equivalent input noise spectrum can be obtained by dividing (21) by the square of the transfer function of the filter given by $H(s)=\boldsymbol{C}(s\boldsymbol{T}_C-\boldsymbol{G})^{-1}\boldsymbol{B}+\boldsymbol{D}$.

Verification and application example

In order to verify the accuracy of the proposed approach a comparison between theoretical results and SPICE simulations has been carried out. The numerical results have been obtained using 4th order Adams-Bashforth's [13] method to integrate differential equation (14) and three-point composite Newton-Cotes quadrature [13] tocalculate coefficients C_n in (16).

For our comparison we use a simple differential-pair transconductor shown in Figure 3. The circuit was implemented in standard 0.35_m AMS technology and simulated using SPICE. The OTA macromodel parameters extracted from the simulations are:
$i_{out}(v_{id})=g_m v_{id}+g_{m3}(v_{id})^3+g_{m5}(v_{id})^5 = 10^{-4}v_{id} - 4.2\cdot10^{-5}(v_{id})^3 - 3.4\cdot10^{-5}(v_{id})^5$ [μA] (v_{id} in volts; accuracy of the series better than 0.1% for v_{id}<0.75V); transconductance g_m=100μA/V; noise parameters (see (18)): $S_w=5.2\cdot10^{-16}$ V·A/Hz, $S_f=2.3\cdot10^{-10}$ V^2.

The OTA circuit in Figure 3 was used to implement the 3rd order Butterworth low-pass filter in a leap-frog (LF) structure shown in Figure 4 (actual filter was implemented in fully differential structure). The element values are: C_1=2.37pF, C_2=2.11pF, C_3=0.79pF; the OTAs in Figure 3 was used as active elements of the filter. 3dB frequency of the filter is 10MHz. Figures 5, 6 and 7 show THD versus frequency with 0.3V input signal amplitude, THD versus input signal amplitude for 5MHz input frequency, and output noise spectrum versus frequency, respectively.

The agreement between theoretical results (line) and SPICE simulation results (point) is very good. It should be emphasized that transient analysis performed by integrating (14) is, due to OTA macromodeling, orders of magnitude faster than the one carried out with transistor level simulation using SPICE.

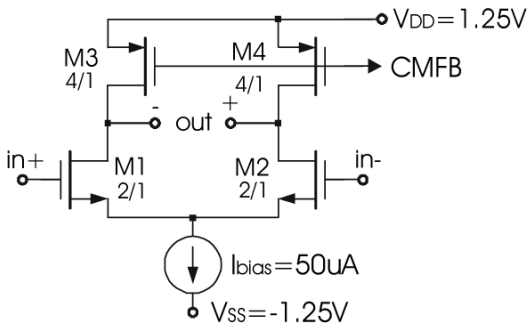

Fig. 3. Simple differential-pair transconductor (Common-Mode Feedback circuit not shown)

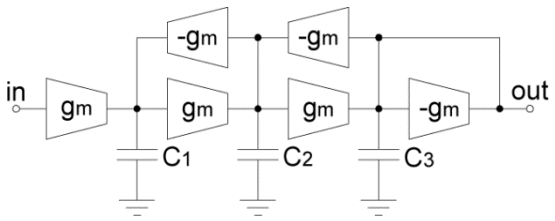

Fig. 4. Diagram of 3rd order LF filter

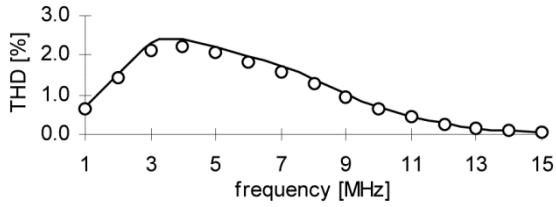

Fig. 5. THD vs. frequency for filter in Figure 4 with 0.3V input amplitude: theoretical data (line), and simulation (points)

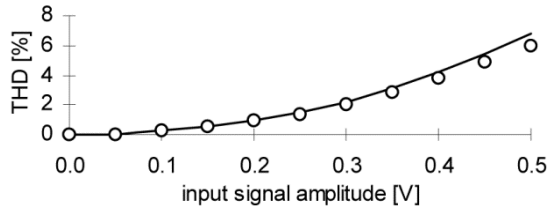

Fig. 6. THD vs. input signal amplitude for filter in Figure 4 with 5MHz sine wave: theoretical data (line), and simulation (points)

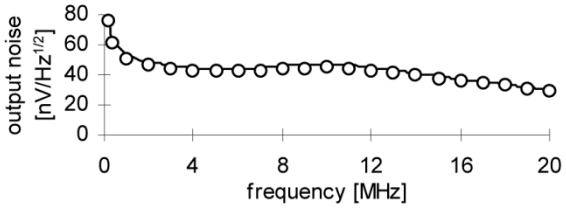

Fig. 7. Output noise spectrum vs. frequency for filter in Figure 4: theoretical data (line), and simulation (points)

As an application example consider performance optimization of 4th order 1dB Chebyshev filter implemented in cascade topology with biquads shown in Figure 8 (actual filter was realized in fully differential structure) and transconductors realized with OTA circuits in Figure 3. Corner frequency of the filter is 10MHz.

In the optimization process we have assumed two degrees of freedom. The first one is biquad ordering (biquad *A* with capacitors C_1=5.65pF, C_2=0.44pF, and biquad *B* with C_1=2.33pF, C_2=3.79pF). The second are biquad gains K_A and K_B. Gains are adjusted by changing transconductance g_b; transconductance g_m=100μA/V is fixed; g_b_[70.7μA/V,141.4μA/V], which allows us to change K_A and K_B in the range of [-3dB,+3dB]. We assumed unity gain setting for the whole filter, i.e. K_A+K_B=0dB.

Note that both nonlinearity and noise parameters of input transcoductors g_b depend on transconductance value, i.e. g_{m3}=g_{m3}(g_b), g_{m5}=g_{m5}(g_b), S_w=S_w(g_b), S_f=S_f(g_b). In this case we modeled them using polynomial approximation, however, we omit the details for the sake of brevity.

Due to the fact that the approach presented in Sections II and III allows us to perform very fast evaluation of nonlinearity and noise parameters of any filter, we were able to perform an exhaustive search through possible biquad configurations (*AB* and *BA*) and gain settings (using small grid of 0.06dB).

Figure 9 shows THD (at 0.6V_{pp} and 2MHz sinusoidal input), Dynamic Range (defined as the ratio of input signal voltage for THD=-40dB@2MHz to the noise integrated over 10MHz pass band), and integrated input noise versus input biquad gain (i.g. K_A for *AB* biquad order and K_B for *BA*).

We can observe that optimal linearity, dynamic and noise performance are obtained for different biquad ordering and gain distribution. Table 1 summarizes best configurations for different optimization criteria. Note that using the proposed approach we were able to obtain full knowledge about the nonlinearity and noise performance of the filter in question and choose the best setting depending on the design priorities.

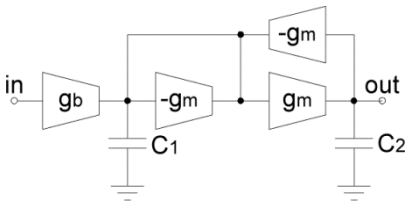

Fig. 8. Diagram of Gm-C biquad

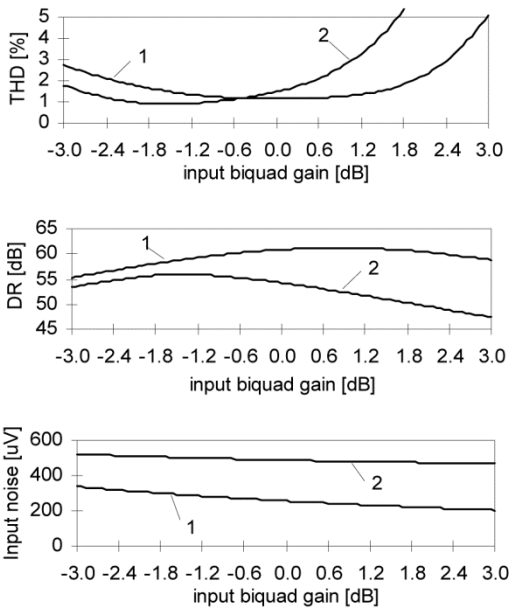

Fig. 9. THD, Dynamic Range (DR), and input integrated noise versus input biquad gain (K_A and K_B for *AB* and *BA* config., respectively) for 4th order cascade Chebyshev filter; configuration *AB* (1), and *BA* (2)

Table 1

Optimal 4th order cascade Chebyshev configuration for best THD, DR and input integrated noise

Optimization Criterion	Best Value	Optimal configuration	
		Biquad Order	Biquad Gains
THD	0.90 [%]	*BA*	K_A=-K_B=1.50 [dB]
DR	61.2 [dB]	*AB*	K_A=-K_B=0.78 [dB]
Integrated noise	204 [μV]	*AB*	K_A=-K_B=3.00 [dB]

Conclusions

A general description of Gm-C filters with nonlinear transconductors including derivation of a differential system describing time evolution of output signal for a general structure of Gm-C filter is formulated. The approach allows us to carry out fast transient analysis and investigate any nonlinear effects in arbitrary Gm-C filter.

The formula for calculating noise of arbitrary Gm-C filter is also developed. The accuracy of the theoretical results is confirmed by comparison to SPICE simulations. It follows that our results have a potential in applying to filter design and optimization, particularly creating effective tools for automated optimizing Gm-C filters with respect to nonlinear distortion and noise performance.

References

[1] R.L. Geiger, E. Sánchez-Sinencio, "Active filter design using operational transconductance amplifiers: A tutorial," *IEEE Circuit and Devices Mag.*, Vol.1, pp.20-32, 1985.

[2] T. Deliyannis, Y. Sun, and J. K. Fidler, *Continuous-time active filter design*, CRC Press, USA, 1999.

[3] B. Nauta, *Analog CMOS filters for very high frequencies*, Kluwer Academic Publishers, 1993.

[4] J. Silva-Martinez, M. Steyaert, W. Sansen, *High-Performance CMOS Continuous-Time Filters*, Kluwer Academic Publishers, Boston/Dordrecht/London, 1993.

[5] Y. Sun (Editor), *Design of high frequency integrated analogue filters*, The Institution of Electrical Engineers, London, 2002.

[6] Y. P. Tsividis, "Integrated continuous-time filter design An overview," *IEEE J. Solid-State Circuits*, vol. 29, pp. 166-176, Mar. 1994.

[7] E. Sánchez-Sinencio and J. Silva-Martinez, "CMOS transconductance amplifiers, architectures and active filters: a tutorial," *IEE Proc.-Circuits Dev. Syst.*, vol. 147, No. 1, pp. 3-12, Feb. 2000.

[8] P. Wambacq, W. Sansen, *Distortion Analysis of Analog Integrated Circuits*, Kluwer Academic Publishers, 1998.

[9] Y. Palaskas, Y. Tsividis, „Dynamic Range Optimization of Weakly Nonlinear, Fully Balanced, Gm-C Filters With Power Dissipation Constraints", *IEEE Trans. Circuits Syst.-II*, Vol.50, No.10, pp.714 -727, Oct.2003.

[10] J. Mahattanakul, C. Bunyakate, „Harmonic injection method: a novel method for harmonic distortion analysis" in *Proc. Int. Symp. Circuits Syst. ISCAS*, Vol.3, pp.85-88, 2001.

[11] S. Koziel, S. Szczepanski, R. Schaumann, "General Approach to Continuous-Time Gm-C Filters," *Int. J. Circuit Theory Appl.*, Vol.31, pp.361-383, July/Aug. 2003.

[12] A. Brambilla, G. Espinosa, F. Montecchi, E. Sánchez-Sinecio, "Noise optimization in operational transconductance amplifier filters," in *Proc. Int. Symp. Circuits Syst. ISCAS*, Vol.1, pp. 118 -121, 1989.

[13] Z. Fortuna, B. Macukow, J. Wasowski, *Metody Numeryczne*, Wydawnictwa Naukowo Techniczne, Warszawa, 1993.

GENERAL STRUCTURE OF INTEGRATOR-BASED CONTINUOUS-TIME ACTIVE-RC FILTER AND APPLICATIONS

Slawomir Koziel,
Faculty of Electronics, Telecommunications and Informatics, Gdansk University of Technology, Gdansk, Poland
koziel@ue.eti.pg.gda.pl

DOI: 10.36724/2664-066X-2021-7-6-8-13

ABSTRACT

In the paper, a general structure of integratorbased continuous-time Active-RC filter is presented. More specifically, filter structures containing inverting amplifiers and passive feedback network are considered. The structure is analyzed using matrix description. The extensions of the model that take into account finite DC gain and finite bandwidth of operational amplifiers as well as other non-ideal effects are presented. The matrix-based approach is formulated especially for efficient use in computer-aidedanalysis and design of Active-RC filters. An application example of the proposed approach to obtain OPAMP specifications for 3rd order low-pass Chebyshev filter for Analog Front End for VDSL is given. In this paper, we consider a general Active-RC filter topology suitable for computer-aided analysis, design and optimization of Active-RC filters. The structure is not the most general one, since it is restricted to filter topologies containing only inverting amplifiers (especially integrators) and RC feedback network.

KEYWORDS: *RContinuous-time filters, Active-RC filters.*

The article is reworked from unpublished 2nd IEEE International Conference on Circuits and Systems for Communications (ICCSC) materials.

Introduction

Continuous-time analog filters based on operational amplifiers (OPAMPs) and RC elements (Active-RC filters) provide solutions for various signal-processing tasks. Many synthesis and design methods for different types and architectures of this class of filters have been reported [1],[2]. Although other techniques, particularly transconductance-capacitor (OTA-C) filters [3], are now dominant in high-frequency range, Active-RC filters are suitable for numerous medium-frequency applications, especially those which require high linearity and low noise, such as ADSL [4], VDSL [5], WCDMA [6],[7], RFIC receivers for PANs [8], GSM baseband transmitters [9]. Recently, an Active-RC filter for frequencies beyond 100MHz has been successfully implemented [10].

In this paper, we consider a general Active-RC filter topology suitable for computer-aided analysis, design and optimization of Active-RC filters. The structure is not the most general one, since it is restricted to filter topologies containing only inverting amplifiers (especially integrators) and RC feedback network. Thus, it is not suitable for analyzing some classical structures such as Sallen-Key biquad [2]. However, it covers a number of practical Active-RC filters, especially most multiple-loop feedback topologies including filters based on RLC ladder simulation, leap-frog, follow-the-leader [1]-[3], and makes it possible to generate and investigate new filter topologies with possibly attractive properties.

Integra-based Active-RC filter structure

Figure 1 shows the single-ended version of the general topology of integrator-based Active-RC filter. The filter in Fig.1 contains n operational amplifiers denoted as O_i, i=1,...,n, n input resistors R_{bi} and capacitors C_{bi}, i=1,...,n, the set of internal feedback resistors R_{ij} and capacitors C_{ij}, i,j=1,...,n, as well as output summer consisting of amplifier O_o, resistors R_d (direct feedforward path from input), R_{ci}, i=1,...,n and R_o. Output nodes of OPAMPs are denoted as x_i, i=1,...,n. We also use z_i (x_i) to denote voltages at OPAMP input (output) nodes. Any integrator-based Active-RC filter is a particular case of the structure in Fig.1 (after removing unnecessary elements). In this section we assume operational amplifiers to be ideal.

To start the analysis note that the total current flowing into each node z_i, i=1,...,n is zero and the voltage at z_i is also zero, due to assumed ideality of OPAMP. This allows us to write the following equations:

$$y_{bi}U_{in} + \sum_{j=1}^{n} y_{ij}x_j = 0\,, \quad i=1,...,n \tag{1}$$

$$g_o U_{out} + \sum_{j=1}^{n} g_{cj}x_j + g_d U_{in} = 0 \tag{2}$$

where U_{in} and U_{out} denote Laplace transforms of input and output voltages, respectively, and

$$y_{bi}=g_{bi}+sC_{bi}, \quad g_{bi}=1/R_{bi}, \quad i=1,...,n$$

$$g_{ci}=1/R_{ci}, \quad i=1,...n, \quad g_d=1/R_d, \quad g_o=1/R_o \tag{3}$$

$$y_{ij} = g_{ij} + sC_{ij}\,, \quad g_{ij} = 1/R_{ij}\,, \quad i,j=1,...,n \tag{4}$$

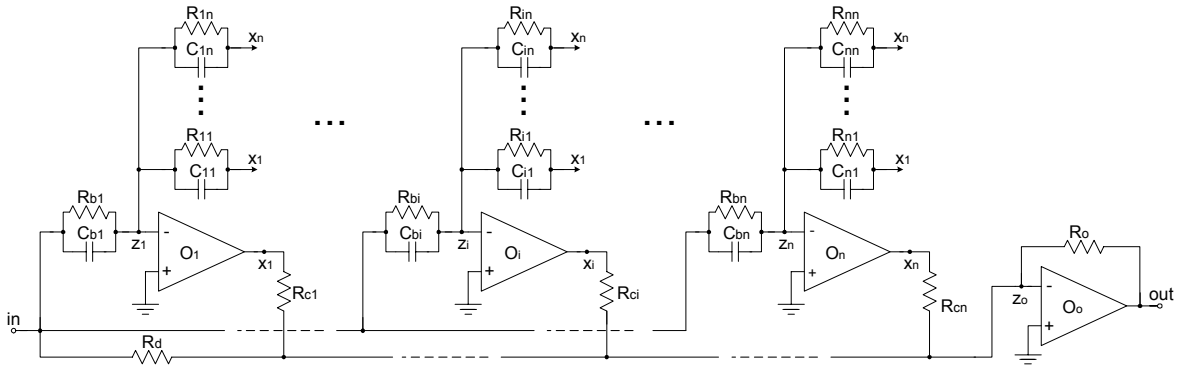

Fig.1. General structure of integrator-based Active-RC filter

Let us introduce the following notation

$$\boldsymbol{T}=\left[C_{ij}\right]_{i,j=1}^{n},\quad \boldsymbol{G}=\left[g_{ij}\right]_{i,j=1}^{n},\quad \boldsymbol{X}=\left[x_1\ \ \cdots\ \ x_n\right]^T$$
$$\boldsymbol{C}=\left[c_1\ \ \cdots\ \ c_n\right]=\left[g_{c1}/g_o\ \ \cdots\ \ g_{cn}/g_o\right],\qquad (5)$$
$$\boldsymbol{B}=\left[g_{b1}+sC_{b1}\ \ \cdots\ \ g_{bn}+sC_{bn}\right]^T,\quad \boldsymbol{D}=d=g_d/g_o$$

Using (5) we can rewrite (1), (2) in the following form

$$\left(s\boldsymbol{T}+\boldsymbol{G}\right)\boldsymbol{X}+\boldsymbol{B}U_{in}=0\qquad U_{out}+\boldsymbol{C}\boldsymbol{X}+\boldsymbol{D}U_{in}=0\quad (6)$$

This allows us to calculate the transfer function $H(s)$ of the filter

$$H(s)=U_{out}(s)/U_{in}(s)=\boldsymbol{C}\left(s\boldsymbol{T}+\boldsymbol{G}\right)^{-1}\boldsymbol{B}-\boldsymbol{D}\qquad (7)$$

Now, let us denote adjoint matrix of $s\boldsymbol{T}+\boldsymbol{G}$ as $\boldsymbol{A}$ where

$$\boldsymbol{A}(s)=adj\left(s\boldsymbol{T}_C+\boldsymbol{G}\right)=\left[A_{ij}(s)\right]_{i,j=1}^{n}\qquad (8)$$

This allows us to rewrite transfer function in the form:

$$H(s)=\frac{1}{\det\left(s\boldsymbol{T}+\boldsymbol{G}\right)}\sum_{i,j=1}^{n}c_i\left(g_{bj}+sC_{bj}\right)A_{ij}(s)-d\qquad (9)$$

Note that in many filter structures, input signal is provided to only one internal node, say z_k (i.e. there is no input signal distribution), and there is no output summer (i.e. one of the internal nodes, say x_l, is the output of the filter), and no input capacitors. This means that $\boldsymbol{B}=\left[0\ \cdots\ 0\ \ g_{bk}\ \ 0\ \cdots\ 0\right]^T$, $\boldsymbol{C}=\left[0\ \cdots\ 0\ -1\ 0\right]\cdots\ 0$

with 1 at l-th position and $C_{bi}=0$ for $i=1,...n$ (note that we have -1 because of the fact that if there is no output summer, there is no signal inversion due to O_o either). In such a case, expression (9) reduces to the form:

$$H(s)=-g_{bk}A_{lk}(s)/\det\left(s\boldsymbol{T}+\boldsymbol{G}\right)\qquad (10)$$

Similar expression can be written for more general cases.

On the basis of the above expressions one can easily calculate the transfer function of any particular structure of integrator-based Active-RC filter. It is also worth noting that there is one-to-one correspondence between integrator-based Active-RC filters and matrices (5). Thus, using presented matrix description we can consider filter design, analysis and optimization in purely algebraic domain. The main advantage is that this can be easily handled by a suitable computer software.

It follows that the order n_H of transfer function of general filter structure in Fig.1 is not necessarily equal to the number of internal nodes. It can be shown that it essentially depends on the passive network. In particular, we have that n_H is not larger than the rank of the corresponding matrix $\boldsymbol{T}$.

Based on the algebraic properties of the matrix $\boldsymbol{T}$, we can distinguish an important subclass of integrator-based Active-RC filters, i.e. state-space filters. If the matrix $\boldsymbol{T}$ is invertible, i.e. $\boldsymbol{T}^1$ exists. Then we can rewrite (6) as

$$s\boldsymbol{X}=-\boldsymbol{T}^{-1}\boldsymbol{G}\boldsymbol{X}-\boldsymbol{T}^{-1}\boldsymbol{B}U_{in}\qquad U_{out}=-\boldsymbol{C}\boldsymbol{X}-\boldsymbol{D}U_{in}\quad (11)$$

Let us denote

$$\boldsymbol{A}_s=-\boldsymbol{T}^{-1}\boldsymbol{G},\ \ \boldsymbol{B}_s=-\boldsymbol{T}^{-1}\boldsymbol{B},\ \ \boldsymbol{C}_s=-\boldsymbol{C},\ \ \boldsymbol{D}_s=-\boldsymbol{D}\quad (12)$$

With this notation (11) takes the form

$$s\boldsymbol{X}=\boldsymbol{A}_s\boldsymbol{X}+\boldsymbol{B}_s\boldsymbol{U}_{in}\qquad U_{out}=\boldsymbol{C}_s\boldsymbol{X}+\boldsymbol{D}_sU_{in}\qquad (13)$$

which is the state-space description of the filter in Figure 1 with node voltages x_i, $i=1,...,n$ being the state variables. Thus, the state-space Active-RC filter is the one for which the matrix $\boldsymbol{T}$ is invertible which is a necessary and sufficient condition for the existence of the state matrices.

For state-space filters we can apply many useful matrix transformations which can be used, for example, to perform efficient parameter optimization [11].

In practice Active-RC filters are mostly implemented in fully differential structures. Due to this we may assume that matrix entries in (5) can take both positive and negative values, which can be accomplished by cross-coupling of corresponding physical elements. More specifically, if the element, say R_{ij}, is cross-coupled (i.e. put between positive [negative] output of an amplifier and positive [negative] input of another one, see e.g. resistor R_1 in Fig.2), this reflects in equation (1) so that the appropriate term has the form $g_{ij}(-x_j)=-g_{ij}x_j$, i.e. the original '-' from node voltage is moved into filter element, here g_{ij}. Obviously, the physical element remains positive. Negative value of the corresponding matrix entry is equivalent to cross-coupling. In case of single-ended implementation, negative elements must be realized using inverters.

The presented approach is primarily intended to be used as a basis for creating computer-aided design and optimization software. However, let us consider a simple example as an illustration how it can be used for hand design. Suppose that we want to synthesize an all-pole biquad filter, i.e. implement the transfer function:

$$H(s)=\frac{H_o\omega_0^2}{s^2+\left(\omega_0/Q\right)s+\omega_0^2}\qquad (14)$$

If one wants to develop minimal implementation, two OPAMPs are needed, so we have $n=2$ in formulas (1)-(9). Assume that our filter has no input signal distribution with input signal injected to the first OPAMP through conductance g_b, i.e. $\boldsymbol{B}=[g_b\ 0]^T$, and no output summer with output signal taken from the second OPAMP, i.e. $\boldsymbol{C}=[0\ -1]$ and $\boldsymbol{D}$. Now we have to choose matrices $\boldsymbol{T}$ and $\boldsymbol{G}$ having in mind that in our case the transfer function of the filter is given by (10). More specifically, denominator of the transfer function is just $\det(s\boldsymbol{T}+\boldsymbol{G})$, while its numerator is $g_bA_{21}(s)$, where $A_{21}(s)=-[s\boldsymbol{T}+\boldsymbol{G}]_{21}$, i.e. element $_{21}$ of the matrix $s\boldsymbol{T}+\boldsymbol{G}$ (multiplied by -1). There are still many possibilities, but the simplest choice is

$$\boldsymbol{T}=\begin{bmatrix}C_1 & 0\\ 0 & C_2\end{bmatrix},\qquad \boldsymbol{G}=\begin{bmatrix}0 & -g_1\\ g_2 & g_3\end{bmatrix}\qquad (15)$$

which gives all-pole second-order transfer function:

$$H(s)=\frac{g_bg_2}{s^2C_1C_2+sC_1g_3+g_1g_2}=\frac{g_bg_2/C_1C_2}{s^2+s\,g_3/C_2+g_1g_2/C_1C_2}\qquad (16)$$

Corresponding filter topology (in fully differential structure) is shown in Fig.2. Obviously, we can obtain many more equivalent filter topologies that implement transfer function (14) by different choice of matrices $\boldsymbol{T}$, $\boldsymbol{G}$, $\boldsymbol{B}$, $\boldsymbol{C}$ and $\boldsymbol{D}$.

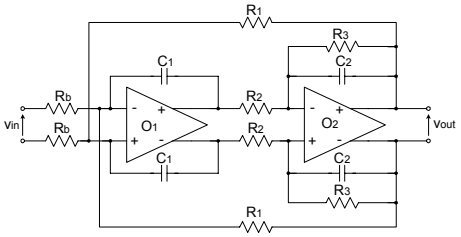

Fig.2. Active-RC biquad corresponding to matrices (15)

III. Active-RC filter with non-ideal OPAMPs

In this section we extend the model presented above to take into account non-ideal behavior of OPAMPs. We shall consider finite gain-bandwidth product of OPAMP as well as its non-zero output resistance. In case of finite gain of OPAMP we can no longer assume that node voltages z_i, i=1,...,n are equal to zero. Denote the gain of i-th operational amplifier O_i as $A_i(s)$ as shown in Fig.3.

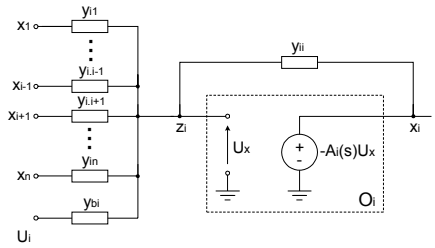

Fig.3. i-th integrator of the filter in Fig.1 with finite gain OPAMP

It follows from Fig.3 that i-th integrator of the filter can be described by the equations:

$$y_{bi}\left(U_{in}-z_i\right)+\sum_{j=1}^{n} y_{ij}\left(x_j-z_i\right)=0 \quad i=1,...,n \qquad (17)$$
$$x_i=-z_i A_i(s)$$

The corresponding equations for the output summer are

$$g_o\left(U_{out}-z_o\right)+\sum_{j=1}^{n} g_{cj}\left(x_j-z_o\right)+g_d\left(U_{in}-z_o\right)=0 \qquad (18)$$
$$U_{out}=-z_o A_o(s)$$

where $A_o(s)$ is the gain of the operational amplifier O_o. Equations (17) and (18) can be rewritten in matrix form:

$$\left(s\boldsymbol{T}+\boldsymbol{G}+\boldsymbol{Y}_A\right)\boldsymbol{X}+\boldsymbol{B}U_{in}=0 \quad \left(1+C_A\right)U_{out}+\boldsymbol{C}\boldsymbol{X}+\boldsymbol{D}U_{in}=0 \qquad (19)$$

where

$$\boldsymbol{Y}_A=\begin{bmatrix}\left(\sum_{j=1}^{n}\bar{y}_{1j}+\bar{y}_{b1}\right)/A_1(s) & & 0\\ & \ddots & \\ 0 & & \left(\sum_{j=1}^{n}\bar{y}_{nj}+\bar{y}_{bn}\right)/A_n(s)\end{bmatrix} \qquad (20)$$

$$C_A=\left(1+\sum_{j=1}^{n}\bar{c}_j+\bar{d}\right)/A_o(s) \quad (C_A=0 \text{ if there is no output summer}) \qquad (21)$$

Here, $\bar{y}_{bi}=|g_{bi}|+s|C_{bi}|$, $\bar{y}_{ij}=|g_{ij}|+s|C_{ij}|$, $\bar{c}_i=|c_i|$, i,j=1,...,n, $\bar{d}=|d|$, which allows us to take into consideration the case when some entries of the matrices $\boldsymbol{T}$, $\boldsymbol{G}$, $\boldsymbol{B}$, $\boldsymbol{C}$, $\boldsymbol{D}$ are negative. In such a case (which is equivalent to cross-coupling of the corresponding physical elements), negative sign of the element value corresponds in fact to the negative sign of appropriate node voltage x_j (see discussion in Section 2). However, from the point of view of input node voltage z_i element is still positive and we must take absolute value of negative elements to maintain correctness of equations. Using (19) we can calculate transfer function of the filter, which is:

$$H(s)=\left(1+C_A\right)^{-1}\left(\boldsymbol{C}\left(s\boldsymbol{T}+\boldsymbol{G}+\boldsymbol{Y}_A\right)^{-1}\boldsymbol{B}-\boldsymbol{D}\right) \qquad (22)$$

Note that even if $A_i(s)$ is modeled using single pole approximation, matrix elements of $\boldsymbol{Y}_A$ are, in general, of second order in s. This makes it difficult to directly evaluate the transfer function formula (22). However, if for frequencies of operation of the filter we have $|A_i(s)|>>1$, i=1,...,n, $|A_o(s)|>>1$, which means that $\|\boldsymbol{Y}_A\|<<\|s\boldsymbol{T}+\boldsymbol{G}\|$ for any reasonable matrix norm, we can use the approximation $(\boldsymbol{I}+\boldsymbol{A})^{-1}\approx\boldsymbol{I}-\boldsymbol{A}$ which is valid for any matrix $\boldsymbol{A}$ as far as $\|\boldsymbol{A}\|<<\|\boldsymbol{I}\|$ ($\boldsymbol{I}$ stands for an identity matrix). Using this we obtain the following formula:

$$H(s)\cong\left(1+C_A\right)^{-1}H_0(s)-\Delta H(s) \qquad (23)$$

where $H_0(s)$ is the nominal transfer function of the filter with ideal OPAMPs (cf. (7)), and $\Delta H(s)$ is deviation from $H_0(s)$ due to finite OPAMP gains given by

$$\Delta H(s)=\left(1+C_A\right)^{-1}\boldsymbol{C}\left(s\boldsymbol{T}+\boldsymbol{G}\right)^{-1}\boldsymbol{Y}_A\left(s\boldsymbol{T}+\boldsymbol{G}\right)^{-1}\boldsymbol{B} \qquad (24)$$

Now, we shall consider the effect of non-zero output impedance of the filter OPAMPs. Fig.4 shows i-th OPAMP of the filter, where $y_{oi}=1/z_{oi}$ denotes its output admittance, $\tilde{x}$ and x_i are the internal and external output voltages of the OPAMP, respectively.

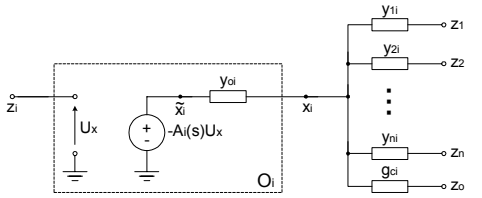

Fig.4. Diagram of *i*-th OPAMP of the filter in Fig.1 with non-zero output admittance

Since in practice we always have $|z_j|<<|x_i|$, $i,j=1,...,n$, we can write the following equation:

$$(\tilde{x}_i - x_i)y_{oi} = x_i\left(|g_{ci}| + \sum_{j=1}^{n}\bar{y}_{ji}\right), \quad i=1,...,n \tag{25}$$

where we wrote $|g_{ci}|$ and $\bar{y}_{ji}$ for the same reason as in (20). Hence, we have

$$x_i = \tilde{x}_i \frac{y_{oi}}{y_{oi} + |g_{ci}| + \sum_{j=1}^{n}\bar{y}_{ji}}, \quad i=1,...,n \tag{26}$$

This means that effective gain of the amplifier is reduced by the factor $\left(1 + z_{oi}\left(|g_{ci}| + \sum_{j=1}^{n}\bar{y}_{ji}\right)\right)^{-1}$, which is, in general, frequency dependent. In order to take it into account output in our previous formulas, we have to replace $A_i(s)$ in (21) by $\tilde{A}_i(s)$ given by

$$\tilde{A}_i(s) = A_i(s)\Big/1 + z_{oi}\left(|g_{ci}| + \sum_{j=1}^{n}\bar{y}_{ji}\right) \tag{27}$$

In a similar way, one can treat output impedance of O_o - OPAMP of the output summer of the filter. We have

$$\left(\tilde{U}_{out} - U_{out}\right)y_o = U_{out}|g_o|, \tag{28}$$

where $\tilde{U}_{out}$ and U_{out} are internal and external output voltages of O_o, while $y_o=1/z_o$ is its output admittance. Hence, we get

$$U_{out} = \tilde{U}_{out}\, y_o/(y_o + |g_o|), \tag{29}$$

which results in replacing $A_o(s)$ in (20) by $\tilde{A}_s^o(\,)$:

$$\tilde{A}_o(s) = A(s)/(1 + z_o|g_o|) \tag{30}$$

IV. Application example

As an application example of the proposed model we shall obtain OPAMP specifications for 3rd order low-pass 1dB Chebyshev filter (3dB frequency equal to 12MHz) for VDSL Analog Front End [5]. Design specifications for VDSL filters are very tough, especially with respect to noise and linearity. Here, we are merely interested in transfer function distortion due to finite gain-bandwidth product and output resistance of filter OPAMPs. We shall consider leap-frog topology shown in Fig.5. We assume that all resistors in the filter are the same and equal to the common value R. We aim at estimating required OPAMP gain-bandwidth product (GBW) and output resistance r_o so that distortion of the filter transfer function due to these non-idealities is within acceptable range.

Fig.6 shows ideal frequency response of the filter in Fig.5, and the response for GBW of OPAMP equal to 200MHz and r_o/R=0.5. We can observe both amplitude distortion (picking) ΔA and 3dB frequency error Δf_{3dB}. Figs.7 and 8 show ΔA and Δf_{3dB}, respectively, versus GBW of OPAMP, for different values of the ratio r_o/R. All the results have been obtained in a single run of the Matlab program implementing formulas presented in Sections II and III. It is seen that Δf_{3dB} is not a big problem since its value is relatively small and can be easily compensated by calibration. However, ΔA is large and heavily dependent on both GBW and r_o/R.

Table 1 shows the value of GBW required to keep ΔA<2dB for different r_o/R ratios. The data in Table 1 represents trade-off between GBW and r_o of the OPAMP. Although we can relax requirements concerning GBW it is always at the expense of decreasing r_o/R ratio. It is not possible to keep this ratio small just by increasing resistor value R because this results in increasing filter noise, which is undesirable. Thus, we have an alternative: either try to obtain large GBW or decrease OPAMP output resistance (this, however, influences OPAMP architecture - very small values of r_o can only be obtained using output buffer which, in turn, degrades both circuit linearity and frequency performance). Discussion of this problem is, however, beyond the scope of this paper. Our goal was just to estimate GBW and r_o/R for which the transfer function distortion is under desired level.

Table 1. OPAMPs GBW ensuring ΔA<2dB of the filter in Fig.5

r_o/R	0	0.25	0.5	1.0	1.5
GBW [MHz]	165	350	550	970	1400

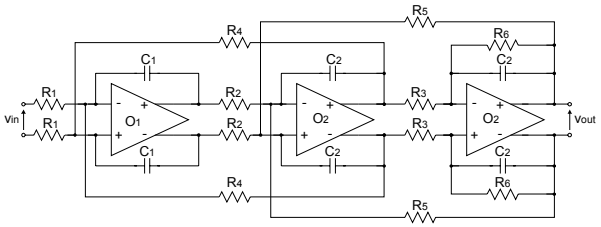

Fig.5. Fully differential 3rd order leap-frog Active-RC filter

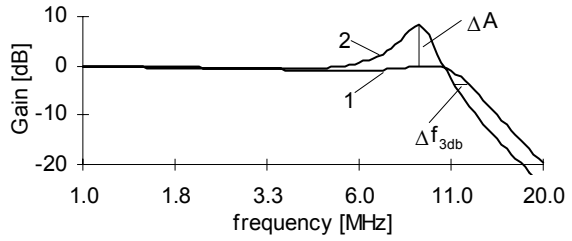

Fig.6. Transfer function distortion of the filter in Fig.5 due to finite OPAMP GBW and r_o; ideal (1) and actual (2) response

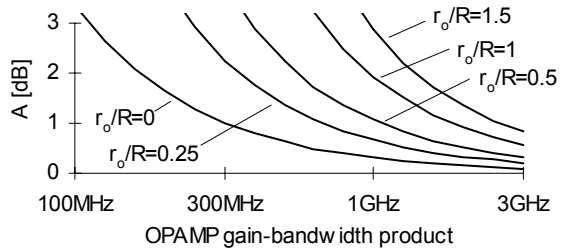

Fig.7. Amplitude distortion ΔA versus GBW of filter OPAMPs for different values of r_o/R ratio

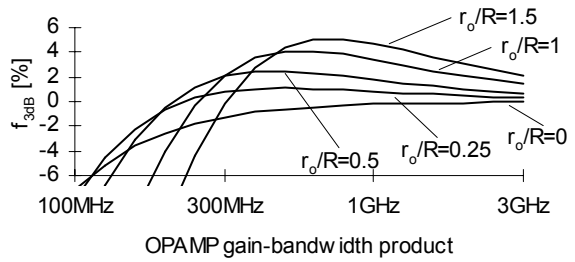

Fig.8. Corner frequency error Δf_{3dB} versus GBW of filter OPAMPs for different values of r_o/R ratio

V. Conclusions

A general structure of integrator-based Active-RC filter is introduced and analyzed using algebraic description. As a result, a matrix-based framework for creating efficient computer-aided analysis and design tools for Active-RC filters is developed. The goal of the future work is to develop, within the presented approach, tools for evaluating noise and nonlinear effects in Active-RC filters and use them in automated design/optimization system.

References

[1] R. Schaumann, M. S. Ghausi, and K. R. Laker, *Design of Analog Filters, Passive, Active RC, and Switched Capacitor*. Englewood Cliff, NJ: Prentice-Hall, 1990.

[2] K. Su, *Analog Filters*, Kluwer Academic Publishers, 2002.

[3] Y. Sun (Editor), *Design of high frequency integrated analogue filters*, The Institution of Electrical Engineers, London, 2002.

[4] S.-S. Lee, „Integration and System Design Trends of ADSL Analog Front Ends and Hybrid Line Interfaces", *Proc. IEEE Custom Integrated Circuits Conf.*, pp.37-44, 2002.

[5] H. Weinberger, A. Wiesbauer, M. Clara, C. Fleischhacker, T. Potscher, B. Seger, „A 1.8V 450mW VDSL 4-Band Analog Front End IC in 0.18µm CMOS", *Proc. IEEE Solid-State Circuits Conf. ISSCC*, Vol.1, pp.326-471, 2002.

[6] J. Jussila, K. Halonen, „A 1.5 V active RC filter for WCDMA applications", *Proc. IEEE Int. Conf. Electronics Circuits. Syst. ICECS*, Vol.1, pp.489-492, 1999.

[7] W. Khalil, T.-Y. Chang, X. Jiang, S.R. Naqvi, B. Nikjou, J. Tseng, „A highly integrated analog front-end for 3G", *IEEE J. Solid-State Circuits*, Vol.38, pp.774-781, 2003.

[8] C. Frost, G. Levy, B. Allison, „A CMOS 2MHz self-calibrating bandpass filter for personal area networks", *Proc. Int. Symp. Circuits Syst. ISCAS*, Vol.1, pp.485-488, 2003.

[9] C.S. Wong, „A 3-V GSM baseband transmitter", *IEEE J. Solid-State Circuits*, Vol.34, pp.725-730, 1999.

[10] J. Harrison, N. Weste, „350MHz opamp-RC filter in 0.18µm CMOS", *Electron. Lett.*, Vol.38, pp.259-260, 2002.

[11] S. Koziel, S. Szczepanski, R. Schaumann, „General Approach to Continuous-Time G_m-C Filters", *Int. J. Circuit Theory Appl.*, Vol.31, pp.361-383, July/Aug. 2003.

THE CONTROLLABILITY OF RLCM NETWORKS OVER F(Z) AND THEIR APPLICATIONS

Xiao-Yu Feng
Wuhan University of Technology, Dept. of Electronic and Information Engineering, Wuhan, China
feng1960@public.wh.hb.cn

Kai-Sheng Lu
Wuhan University of Technology, Dept. of Marine Automation, Wuhan, China
kashlu@wuhan.cngb.com

DOI: 10.36724/2664-066X-2021-7-6-14-20

ABSTRACT

The subject of controllability and observability in dynamical systems is one of the important matters in linear system theory. The controllability and observability in linear systems over the field R of real numbers were heavily studied. If the values of resistors, capacitors, and self and mutual inductors in RLCM network are regard as independently variable parameters, the network is defined over the field F(z) of all rational functions in its physical parameters. Some concepts and results on the reducibility and separability for this network are presented; the controllability problem and application are discussed. In this paper the author will discuss the relationship between separability and reducibility of RLCM networks over F(z), the relationship between the physical structure of RLCM networks and structural controllability. The results in this paper can be used to study different kinds of linear or nonlinear electrical networks (over F(z)).

KEYWORDS: *RLCM networks over F(z), Controllability, Reducibility, Separability.*

The article is reworked from unpublished 2nd IEEE International Conference on Circuits and Systems for Communications (ICCSC) materials.

Introduction

The subject of controllability and observability in dynamical systems is one of the important matters in linear system theory. The controllability and observability in linear systems over the field R of real numbers were heavily studied. However, uncontrollability (unobservability) is a "singular" condition in the sense that if the system $\dot{X}$ =AX+Be, Y=CX+De is uncontrollable (unobservable), then almost any small perturbation of the elements of A and B (A and C) will cause it to become controllable (observable) [1]. Why does it happen? When the effect of the values of elements in A and B (A and C) is excluded? What is the independent of effect of its structure? In order to analyze the issue and explore the independent of system structures and structural controllability, many researchers proposed various parametrizations [2-11].

Let F(z) denote the field of all rational functions with real coefficients in q independently variable parameters $z_1,\ldots, z_q$. Let $z=(z_1 ,\ldots, z_q)$. The domain of z is R^q and R^q is also said to be the parameter space. Let F(z)[s] denote the ring of all F(z)-coefficient polynomials in s. A matrix M is called a rational function matrix (RFM) or a matrix over F(z) if each entry of the matrix is a member of F(z). A linear system is a rational function system (RFS) or a system over F(z) if all coefficient matrices A, B, C and D of the system are RFMs. For example, if all physical parameters (resistors, capacitors, self and mutual inductors) of an RLCM network-a network consisting of resistors, capacitors, and self and mutual inductors, are considered to be mutually independently variable parameters, then all coefficient matrices of the network are RFMs and it is an RFS or an RLCM network over F(z).

The field R of real numbers is a subfield of F(z) and the controllability over F(z) is equivalent to structural controllability (see Section 2). Thus, the controllability of the systems over F(z), that is, structural controllability, is more universal. The systems over R can be a class of systems over F(z).

For a physical system with given structure such as an RLCM network with given topology, its coefficient matrices A, B, C and D are ones over R and it is a system over R only if its parameter values (ie., the values of its resistors, capacitors, and self and mutual inductors) are given. So, the controllability and observability of the system over R depend on both its physical structure and parameter values. If all physical parameters of the system are regarded as mutually independently variable parameters, not as real constants, then it is a system over F(z). The controllability of the system over F(z) is independent of the values of its physical parameters because the values of *z* have never been given for the controllability of the system over F(z). So the effect of the parameter values is excluded, and only that of the physical structure is left. Therefore the controllability over F(z) is just the structural controllability of the physical system.

In this paper the author will discuss the relationship between separability and reducibility of RLCM networks over F(z), the relationship between the physical structure of RLCM networks and structural controllability. Example 7.1 in Section 7 shows that analyzing the controllability of RLCM systems over F(z) may be significant from the viewpoint of physics. The results in this paper can be used to study different kinds of linear or nonlinear electrical networks (over F(z)).

Preliminaries

Consider a linear system over F(z)

$$\dot{X} =AX+Be，Y=CX+De， \qquad (2\text{-}1)$$

Where A,B,C and D are, respectively, n×n, n×m, p×n, and p×m matrices, $X \in R^n$, $U \in R^g$, $Y \in R^e$ and RES(2-1) has q variable parameters $z=(z_1, z_2, \ldots, z_n, z_{n+1}, \ldots, z_q) \in R^q$. Let T=[sI-A,B] and $T_0=[sI-A', C']'$. Let

$M=\{z \in R^q \mid \text{rank}T=n, \ \forall s \in \hat{C}\}$ or
$M=\{z \in R^q \mid \det(T\overline{T}) \neq 0, \ \forall s \in \hat{C}\}$,
$N=\{z \in R^q \mid \text{rank}T_0=n, \ \forall s \in \hat{C}\}$ or
$N=\{z \in R^q \mid \det(T_0\overline{T_0}) \neq 0, \forall s \in \hat{C}\}$,

where $\hat{C}$ denotes complex field, T and $\overline{T_0}$ are complex conjugate of T and T_0 respectively. Let S be a point set and m*S denote the Lebesgue measure of the set S.

Definition 1. RES(2-1) is structurally controllable (SC) if m*M=1; otherwise, it is not SC. RES(2-1) is structurally observable (SO) if m*N=1; otherwise, it is not SO.

Definition 2. RES(2-1) is controllable over F(z) or it is controllable for short if $\det(T\overline{T})$ is nonzero member of F(z) for $\forall s \in \hat{C}$; otherwise, it is uncontrollable. RES(2-1) is observable over F(z) or it is observable for short if $\det(T_0\overline{T_0})$ is a nonzero member of F(z) for $\forall s \in \hat{C}$; otherwise, it is unobservable.

Lemma 1. Let $f(z) \in F(z)$. If f(z) is a zero member of F(z) (simply f(z)=0), then f(z)=0 for all $z \in R^q$; if f(z) is a nonzero member of F(z) (simply $f(z) \neq 0$), $m^*\{z \in R^q \mid f(z) \neq 0\}=1$.

Remark 1. By the above Definitions and Lemma 1. SC(SO) is equivalent to the controllability

Let A be an n×n matrix over F(z), A is said to be reducible under $P_1AP_1^{-1}$ or simply to be reducible if there exists some nonsingular matrix P_1 over F(z) such that

$$P_1AP_1^{-1}=\begin{pmatrix} A_1 & 0 \\ A_{21} & A_2 \end{pmatrix}, \qquad (2\text{-}2)$$

where A_i is an $n_i \times n_i$ matrix, i=1,2, $1 \leqslant n_i < n$; otherwise A is irreducible. A is said to be reducible under PA P' if there exists some permutation matrix P such that

$$PAP'=\begin{pmatrix} A_1 & 0 \\ A_{21} & A_2 \end{pmatrix}, \qquad (2\text{-}3)$$

where A_i is an $n_i \times n_i$ matrix, i=1,2, $1 \leqslant n_i < n$; otherwise, A is irreducible under PA P'.

Reducibility condition

Corollary 3.1: Let $K \subseteq F$ be field, $A=(V+W)^{-1}T$, where $V=\text{diag}[\zeta_1, \ldots, \zeta_n]$ is a matrix over F such that $\zeta_1, \ldots, \zeta_n$ are algebraically independent over the field K, W with indeterminates $\alpha_1,\ldots,\alpha_{m1}$ and T with indeterminates $\beta_1,\ldots,\beta_{m2}$ are two n×n matrices over K, $z=(\zeta_1, \ldots, \zeta_n, \alpha_1,\ldots,\alpha_{m1}, \beta_1,\ldots,\beta_{m2})$, and T is invertible, then the following propositions are equivalent.

1. A is an n×n irreducible matrix over F(z) (or det (λI-A) is irreducible).
2. A is an n×n irreducible matrix under PA P' over F(z).

Proof: This proof is obvious by Theorem 3 and Corollary 3 in [11].

Corollary 3.2: Let $K \subseteq F$ be field, $A=(V+W)^{-1}T$, where $V=\text{diag}[\zeta_1, \ldots, \zeta_n]$ is a matrix over F such that $\zeta_1, \ldots, \zeta_n$ are algebraically independent over the field K, W and T are two n×n matrices over K, then there exist some permutation P such that A is reducible under PA P' iff there exist some permutation P_1 such that $H=[s(V+W)-T]$ is reducible under P_1HP_1', where s is a parameter independent of $\zeta_1, \ldots, \zeta_n$.

Proof: Since $A=(V+W)^{-1}T$, then by Theorem 3 in [11], A is irreducible under PA P' iff [V+W-Tt] is irreducible under $P_1[V+W-Tt]$ P_1'. Moreover $H=[s(V+W)-T]= s(V+W-Tt)$, $t=s^{-1}$, the reducibility of H is equivalent to the reducibility of (V+W-Tt). Hence, this corollary is true.

Controllability (observability) Criteria

Theorem 4.1: A is an n×n irreducible matrix over F(z), the equation (2-1) is controllable (observable) over F(z) iff B 0 (C≠0)

Proof: we shall first proof the controllability.

Necessity: it is obvious that if B=0, then (2-1) is uncontrollable

Sufficiency: since A is irreducible and B 0, then rank[sI-A, B]=n at every eigenvalue of A. if not, then there exist an eigenvalue λ and a 1×n vector α 0 such that

$$\alpha[\lambda I-A,B]=0 \quad \text{or} \quad \alpha\lambda=\alpha A \text{ and } \alpha B=0$$

which imply $\alpha A^2=\lambda\alpha A=\lambda^2\alpha$
and in general, $\alpha A^i=\lambda^i\alpha$ i=1,2,…
Let $T=[B \ AB \ \ldots \ A^{n-1}B]$ is the controllability matrix, hence we have

$$\alpha T=[\alpha B \ \lambda\alpha B \ \ldots \ \lambda^{n-1}\alpha B]=0$$

which means rankT=k<n.. Then by Theorem 1 in [12], there exists some n×n nonsingular matrix P over F(z) such that

$$[\bar{A},\bar{B}]=[P^{-1}AP,P^{-1}B]=\begin{pmatrix} A_c & 0 & 0 \\ A_{21} & A_c & B_c \end{pmatrix}$$

which is contradicts the fact that A is irreducible. So rank[sI-A, B]=n. This implies that (A,B) is controllable, that is, the equation (2-1) is controllable over F(z).

the equation (2-1) is observable over F(z) iff C 0, because the observability and controllability are coupled.

Relationship between Separability and Reducibility

Definition 3. A graph is said to be separable (hinged) if there is at least one subgraph that has at most one node in common with its complement subgraph in the graph; otherwise it is an unhinged graph. A subgraph in a hinged graph is called an unhinged subgraph if it has at most one node in common with its complement subgraph and it is unhinged. Clearly, there are k unhinged subgraphs in a hinged graph, k⩾2. An RLCM network is separable if its graph is hinged; otherwise, it is unhinged. A subnetwork in a hinged network is unhinged if its graph is an unhinged subgraph. An RLCM network is electrically separable if ① its graph is hinged, there is no mutual coupling between any branch of one unhinged subnetwork and any branch of another unhinged subnetwork; otherwise, it is electrically unhinged.

In order to discuss relationship between separability and reducibility, we should first systematically formulate the state equation of an RLCM network. According to Electrical Network Theory[13], we write KVL equation for the fundamental-loop and KCL equation for the f-cut-set in matrix form:

$$\begin{bmatrix} V_{Cl} \\ V_{Rl} \\ V_{Ll} \\ V_J \end{bmatrix} = \begin{bmatrix} Q'_{EC} & Q'_{CC} & 0 & 0 \\ Q'_{ER} & Q'_{CR} & Q'_{RR} & 0 \\ Q'_{EL} & Q'_{CL} & Q'_{RL} & Q'_{LL} \\ Q'_{EJ} & Q'_{CJ} & Q'_{RJ} & Q'_{LJ} \end{bmatrix} \begin{bmatrix} V_E \\ V_{Ct} \\ V_{Rt} \\ V_{Lt} \end{bmatrix},$$
$$\begin{bmatrix} I_E \\ I_{Ct} \\ I_{Rt} \\ I_{Lt} \end{bmatrix} + \begin{bmatrix} Q_{EC} & Q_{ER} & Q_{EL} & Q_{EJ} \\ Q_{CC} & Q_{CR} & Q_{CL} & Q_{CJ} \\ 0 & Q_{RR} & Q_{RL} & Q_{RJ} \\ 0 & 0 & Q_{LL} & Q_{LJ} \end{bmatrix} \begin{bmatrix} I_{Cl} \\ I_{Rl} \\ I_{Ll} \\ I_J \end{bmatrix} = 0 \qquad (5\text{-}1)$$

where all variables in capital letter are in Laplace -transformed form. $V_{Ct}(I_{Ct})$, $V_{Rt}(I_{Rt})$, $V_{Lt}(I_{Lt})$, $V_{Cl}(I_{Cl})$, $V_{Rl}(I_{Rl})$, $V_{Ll}(I_{Ll})$, $V_E(I_E)$ and $V_J(I_J)$ are n_{Ct}, n_{Rt}, n_{Lt} n_{Cl}, n_{Rl}, n_{Ll}, n_E, and n_J dimentional vector. each element of $V_{Ct}(I_{Ct})$, $V_{Rt}(I_{Rt})$, $V_{Lt}(I_{Lt})$, $V_{Cl}(I_{Cl})$, $V_{Rl}(I_{Rl})$ and $V_{Ll}(I_{Ll})$ corresponds to each diagonal element of C_t, R_t, L_t, C_l, R_l and L_l, for example, $V_{Ct}=[V_{Ct}(1),\ldots,V_{Ct}(n_{Ct})]'$, $C_t=\mathrm{diag}[C_t(1),\cdots,C_t(n_{Ct})$, $V_{Ct}(i)$ is the voltage across $C_t(i)$, $i=1,\cdots,n_{Ct}$.

For RLCM network, we have following voltage-current relations:

$$\begin{bmatrix} I_{Rt} \\ I_{Rl} \end{bmatrix} = \begin{bmatrix} G_t & 0 \\ 0 & G_l \end{bmatrix} \begin{bmatrix} V_{Rt} \\ V_{Rl} \end{bmatrix}, \quad \begin{bmatrix} V_{Lt} \\ V_{Ll} \end{bmatrix} = \begin{bmatrix} sL_t & sM_{tl} \\ sM_{lt} & sL_l \end{bmatrix} \begin{bmatrix} I_{Lt} \\ I_{Ll} \end{bmatrix} = sL \begin{bmatrix} I_{Lt} \\ I_{Ll} \end{bmatrix},$$
$$\begin{bmatrix} I_{Ct} \\ I_{Cl} \end{bmatrix} = \begin{bmatrix} sC_t & 0 \\ 0 & sC_l \end{bmatrix} \begin{bmatrix} V_{Ct} \\ V_{Cl} \end{bmatrix} \qquad (5\text{-}2)$$

In above expressions G_l, G_t, C_l and C_t are the matrices of conductance links and twigs, capacitor links and twigs; they are diagonal. Because of the possibility of mutual inductance, there may be coupling between inductor twigs and links, which means $M_{tl} \neq 0$, as well as between inductor twigs themselves and inductor links themselves, which means M_{ll} and M_{tt} are not zero. So the inductor matrices L are not diagonal, but $L_l=L_{ll}+M_{ll}$ and $L_t=L_{tt}+M_{tt}$ are symmetric, L_{ll} and L_{tt} are diagonal, $M_{ll}=M'_{ll}$, $M_{tt}=M'_{tt}$, $M_{tl}=M'_{lt}$.

From (5-1) and (5-2), we have

$$\begin{bmatrix} s(C_t+Q_{CC}C_lQ'_{CC})+Q_{CR}R^{-1}Q'_{CR} & Q_{CL}-Q_{CR}R^{-1}Q'_{RR}R_tQ_{RL} \\ Q'_{CL}-Q'_{RL}G^{-1}Q_{RR}G_lQ'_{CR} & -s(L_l+Q'_{LL}L_tQ_{LL}-Q'_{LL}M'_{lt} \\ & -M_{lt}Q_{LL})-Q'_{RL}G^{-1}Q_{RL} \end{bmatrix} \begin{bmatrix} V_{Ct} \\ I_{Ll} \end{bmatrix}$$
$$= \begin{bmatrix} -Q_{CR}R^{-1}Q'_{ER}-sQ_{CC}C_lQ'_{EC} & Q_{CR}G_lQ'_{RR}G^{-1}Q_{RJ}-Q_{CJ} \\ Q'_{RL}G^{-1}Q_{RR}G_lQ'_{ER}-Q'_{EL} & Q'_{RL}G^{-1}Q_{RJ}+s(Q'_{LL}L_tQ_{LJ} \\ & -M_{lt}Q_{LJ}) \end{bmatrix} \begin{bmatrix} V_E \\ I_J \end{bmatrix} \qquad (5\text{-}3)$$

where

$G=G_t+Q_{RR}G_lQ'_{RR}$, $R=R_l+Q_{RR}R_tQ'_{RR}$, $G_t^{-1}=R_t$, $G_l^{-1}=R_l$,

$Q'_{CL}-Q'_{RL}G^{-1}Q_{RR}G_lQ'_{CR}=(Q_{CL}-Q_{CR}R^{-1}Q'_{RR}R_tQ_{RL})'$

Suppose that there are no loops containing just capacitors and independent voltage source and there are no cut-sets containing just inductors and independent current sources, which means that $Q_{CC}sC_lQ'_{EC}=0$ and $Q'_{LL}L_tQ_{LJ}-M_{lt}Q_{LJ}=0$. To simplify, define

$$E=\begin{bmatrix} -Q_{CR}R^{-1}Q'_{ER} & Q_{CR}G_lQ'_{RR}G^{-1}Q_{RJ}-Q_{CJ} \\ -Q'_{RL}G^{-1}Q_{RR}G_lQ'_{ER}+Q'_{EL} & -Q'_{RL}G^{-1}Q_{RJ} \end{bmatrix}=\begin{bmatrix} E_{11} & E_{12} \\ E_{21} & E_{22} \end{bmatrix}$$
$$V=\begin{bmatrix} C_t & 0 \\ 0 & L_l \end{bmatrix}, \quad W=\begin{bmatrix} Q_{CC}C_lQ'_{CC} & 0 \\ 0 & Q'_{LL}L_tQ_{LL}- \\ & Q'_{LL}M'_{lt}-M_{lt}Q_{LL} \end{bmatrix},$$
$$T=\begin{bmatrix} -Q_{CR}R^{-1}Q'_{CR} & -Q_{CL}+Q_{CR}R^{-1}Q'_{RR}R_tQ_{RL} \\ Q'_{CL}-Q'_{RL}G^{-1}Q_{RR}G_lQ'_{CR} & -Q'_{RL}G^{-1}Q_{RL} \end{bmatrix}, \qquad (5\text{-}3a)$$

then (5-3) can be written as

$$[s(V+W)-T][V'_{Ct} \quad I'_{Ll}]'=E[V'_E \quad I'_J]' \qquad (5\text{-}4)$$

According to Electrical Network Theory, if an RLCM network contains no perfectly coupled inductors, the principal minors of L will be nonsingular, which implies that $(V+W)^{-1}$ exists, so take the inverse Laplace transform of (5-4), we have

$$\frac{d}{dt}\begin{bmatrix} v_{Ct} \\ i_{Ll} \end{bmatrix} = (V+W)^{-1}T\begin{bmatrix} v_{Ct} \\ i_{Ll} \end{bmatrix} + (V+W)^{-1}E\begin{bmatrix} v_E \\ i_J \end{bmatrix} \qquad (5\text{-}5)$$

This is a matrix differential equation of the first order. Equation (5-5) can be written in compact matrix notation as

$$dx/dt = Ax + Be \qquad (5\text{-}6)$$

where the meaning of the matrices of A, B, *x* and *e* are obvious. Since all the resistors, capacitors, and self and mutual inductors are regarded as mutually independently variable parameters, so from (5-3a), we know that matrix A in (5-6) is similar to matrix A in Corollary 3.1, so we have following conclusion:

Theorem 5.1: RLCM network (5-6), when shorting voltage-sources and opening current-source, ie., *e*=0, is electrically unhinged iff there does not exist any permutation matrix P such that A is irreducible under PA P'.

Proof: Obviously, A is reducible under PA P' if the network (5-6) without sources is electrically hinged (separapable). It is only necessary to prove the necessity.

Since A=$(V+W)^{-1}$T, then by Corollary 3.2, if A is reducible under PA P', there must exist some permutation matrix P_1 such that H= s(V+W)-T is reducible under P_1H P_1', that is

$$P_1HP_1' = \begin{bmatrix} H_1 & 0 \\ 0 & H_2 \end{bmatrix} = P_1\begin{bmatrix} \Psi & \vartheta \\ -\vartheta' & \Phi + s\mathcal{M} \end{bmatrix}P_1' \qquad (5\text{-}7)$$

where H_1 is an γ×γ matrix, $1 \le \gamma < n_{Ct}+n_{Ll}$; all Ψ, ϑ, Φ and $\mathcal{M}$ are not zero,

$$\Psi = s(C_t + Q_{CC}C_l Q_{CC}') + Q_{CR}R^{-1}Q_{CR}',$$
$$\vartheta = Q_{CL} - Q_{CR}G_l Q_{RR}' G^{-1}Q_{RL},$$
$$\Phi = s(L_{ll} + Q_{LL}' L_{tt}Q_{LL}) + Q_{RL}' G^{-1}Q_{RL},$$
$$\mathcal{M} = (M_{ll} + Q_{LL}' M_{tt}Q_{LL} - Q_{LL}' M_{lt}' - M_{lt}Q_{LL}).$$

Clearly, P_1H P_1' will have three kinds of expressions as follows

$$①\begin{bmatrix} \Psi_1 & 0 & 0 \\ 0 & \Psi_2 & \vartheta \\ 0 & -\vartheta' & \Phi + s\mathcal{M} \end{bmatrix},\quad ②\begin{bmatrix} \Psi & \vartheta & 0 \\ -\vartheta' & \Phi_1 + s\mathcal{M}_1 & 0 \\ 0 & 0 & \Phi_2 + s\mathcal{M}_2 \end{bmatrix},$$

$$③\begin{bmatrix} \Psi_1 & \vartheta_1 & & 0 \\ -\vartheta_1' & \Phi_1 + s\mathcal{M}_1 & & \\ & & \Psi_2 & \vartheta_2 \\ 0 & & -\vartheta_2' & \Phi_2 + s\mathcal{M}_2 \end{bmatrix},$$

where Ψ_i, ϑ_i, Φ_i and $\mathcal{M}_i$ are submatrices of Ψ, ϑ, Φ and $\mathcal{M}$, i=1,2. If $\mathcal{M}$=0, which means there are no mutual coupling among the inductor branches, RLCM network will change into RLC network, then by Theorem 3.1 in [14], the network is hinged, there exist at least two unhinged subnetworks. If $\mathcal{M}$ 0, RLCM network will also be hinged because mutual inductance do not influence separability of the network; from above three expressions, we know that there exist at least two subnetworks G_1 relating with matrix H_1 and G_2 relating with matrix H_2, where G_1 and G_2 are unconnected or they have one node in common, expression shows that there are no electrical mutual coupling between G_1 and G_2 because G_1 has no inductor, expression and expression show the same result because there are no mutual inductance between the inductor branches of G_1 and the inductor branches of G_2 (which is caused by the reducibility of $\mathcal{M}$: there exist some permutation P_2 such that $P_2\mathcal{M}P_2'$=diag($\mathcal{M}_1, \mathcal{M}_2$)). So if A is reducible under PA P', then RLCM network is electrically unhinged.

Some results of Controllability

In (5-6), let $\dot{X} = dx/dt$, $X = x$, then we have

$$\dot{X} = AX + Be \qquad (6\text{-}1)$$

where A=$(V+W)^{-1}$T, B=$(V+W)^{-1}$E, (6-1) is same as the first equation of (2-1). By Electrical Network Theory, if the network without source does not contain any independent all-inductor loops or independent all-capacitor cut-sets, T in (5-3a) will be invertible, so according to Theorem 5.1, Corollary 3.1 and Theorem 4.1, we have following result.

Result 1: an electrically unhinged RLCM network (6-1), in which ① there are no loops containing just capacitors and independent voltage source and there are no cut-sets containing just inductors and independent current sources ② there is no independent all-inductor loop or independent all-capacitor cut-set when shorting voltage-sources and opening current-source, is controllable and observable over F(z), i.e., structurally controllable, iff B≠0.

Now let us turn to when B is not zero. B=$(V+W)^{-1}$E, since $(V+W)^{-1}$ is nonsingular matrices, so B≠0 iff E≠0.

By Electrical Network Theory, we know that if there only exist independent voltage sources in the network, we can get the coefficient submatrices E_{11}, E_{21} in the following ways: open all reactive links and short all reactive twigs, then E_{11} is computed by finding the currents i_{11} in the shorted capacitor twigs and E_{21} is computed by finding the voltage v_{21} at the open inductor links, it is impossible that i_{11} and v_{21} are zero simultaneously, so if $v_E \neq 0$, then $E_1=[E'_{11}\ \ E'_{21}]' \neq 0$. In a similar way, we have: if $i_J \neq 0$, then $E_2=[E'_{12}\ \ E'_{22}]' \neq 0$, this means that if there exist the sources in the network, E must not be zero, that is $B \neq 0$. An result is easy to yield as follows

Result 2: an electrically unhinged RLCM network without perfectly coupling inductors, in which ① there are no loops containing just capacitors and independent voltage source and there are no cut-sets containing just inductors and independent current sources ② there is no independent all-inductor loop or independent all-capacitor cut-set when shorting voltage-sources and opening current-source, is always controllable over F(z), i.e., is structurally controllable.

Applications to RLCM networks

Example 7.1. Consider an RLCM network without perfectly coupling as shown in Fig.1.

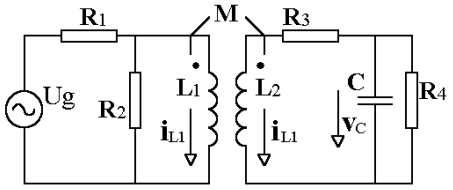

Fig. 1. an RLCM network

Let the state vector be $X=(v_C, i_{L1}, i_{L2})'$ and the input be the voltage source Ug. The state equation of the network is $\dot{X}=AX+Bu$, where

$$A=\frac{1}{\Delta}\begin{bmatrix} \frac{M^2-L_1L_2}{R_4} & 0 & M^2-L_1L_2 \\ -CM & -CL_2(R_1 // R_2) & -CMR_3 \\ CL_1 & CM(R_1 // R_2) & CL_1R_3 \end{bmatrix}, B=\frac{1}{\Delta}\begin{bmatrix} 0 \\ CL_2 \\ -CM \end{bmatrix}$$

$\Delta=C(L_1L_2-M^2)$, $R_1//R_2=R_1R_2/(R_1+R_2)$, $L_1L_2-M^2>0$ (7-1)

Let C, R_1, R_2, R_3, R_4, L_1, L_2, M be eight independently variable parameters (not be eight real constants), i.e., z=(C, R_1, R_2, R_3, R_4, L_1, L_2, M). Then, the network described by (7.1) is not one over R but one over F(z). Look at the physical structure of Fig.1., the network is hinged but is electrically unhinged, so by Result 2, the network is controllable over F(z), i.e., $m^*S=\{z \in R^5 \mid \text{rank}[sI-A,B]=3, \forall\ s \in \hat{C}\}=1$ by Definition 1, obviously, this is dependent only on the network structure.

If $R_1=R_2=2\,\Omega$, $R_3=R_4=1\Omega$, C=1F, L_1=2H, L_2=M=1H, then

$$A=\begin{bmatrix} -1 & 0 & -1 \\ -1 & -1 & -1 \\ 2 & 1 & 2 \end{bmatrix}, B=\begin{bmatrix} 0 \\ 1 \\ -1 \end{bmatrix} \qquad (7\text{-}2)$$

are two matrices over R and the network described by (7-2) is one over R, hence we have

$$[sI-A,B]=\begin{bmatrix} s+1 & 0 & 1 & 0 \\ 1 & s+1 & 1 & 1 \\ -2 & -1 & s-2 & -1 \end{bmatrix},$$

when s=0, then rank[sI-A,B]=2<3, so the network (7-2) over R is uncontrollable, clearly, the result is caused by both the physical parameter values (C, R_1, R_2, R_3, R_4, L_1, L_2, M)= (1, 1, 1, 1, 1, 2, 1, 1) and the structure of the network, because (7-2) is determined by both. $m^*S=\{z\in R^5 \mid \text{rank}[sI-A,B]=3, \forall\ s\in\hat{C}\}=1$ means that the point set $\overline{S}=(z\in R^5 \mid \text{rank}[sI-A,B]<2)$ is a hypersurface in parameter space R^8, it is impossible that a point in parameter space R^8 fall on hypersurface $\overline{S}$ accurately. So when $z=\overline{z}$ =(1, 1, 1, 1, 1, 2, 1, 1)$\in\overline{S}$, then $m^*\overline{S}=0$, which implies that if the values of *z* are at random chosen in the parameter space R^8, then the probability that the network over *R* is controllable is one. This shows that if a network over F(z) is controllable, i.e., structurally controllable, then actually its network over R is always controllable . Therefore, analyzing the controllability of linear physical systems over F(z) is significant from the practical viewpoint.

Acknowledgements

The work described in this paper was fully supported by the National Science Found grant 50177024

References

[1]. E.B.Lee and L.Markus, Foundations of optimal control theory, John Wiley & Sons, New York, 1967.

[2]. C.T.Lin, "Structural controllability," IEEE Trans., AC-19,pp.201-208, 1974.

[3]. K.Glover and L.M.Silverman, "Characterization of structural controllability," IEEE Trans., AC-21, pp.534-537, 1976.

[4]. E.J.Davison, "connectability and structural controllability of composite systems," Automatica, 13, pp.109-123, 1977.

[5]. H.Mayeda, "On structural controllability theorem," IEEE Trans., AC-26, pp.795-798, 1981.

[6]. B.D.O.Anderson and H.M.Hong, "Structural controllability and matrix nets," Int.J.Contro., 35, pp.397- 416, 1982.

[7]. J.L.Willems, "Structural controllability and observability," Syst.Contr.Lett.,8, pp.5-12, 1986.

[8]. K.Murota, "On the degree of mixed polynomial matrices," SIAM J. Matrix Anal. Appl., 20, pp.196-227, 1998.

[9]. K.Murota, Mixed matrices: Irreducibility and decomposition, Springer-Verlag, New-York, 1993.

[10]. K.S.Lu and J.N.Wei, "Rational function matrices and structural controllability and observability," IEE Proc.-D, 138, pp.388-394, 1991.

[11]. K.S.Lu and J.N.Wei, "Reducibility condition of a class of rational function matrices," SIAM J. Matrix Anal.Appl., 15, pp.151-161, 1994.

[12]. K.S.Lu, "the Controllability of Linear Systems over F(z)" IEEE Conference on Decision and Control Orlando, Florida USA, December 2001.

[13]. N.Balabanian and T.A.Bickart, Electrical Network Theory, John Wiley & Sons, New York, 1969.

[14]. K.S.Lu and K.Lu, "Separability and reducibility criteria of RLC networks over F_z and their applications" Int.J.Circuit Theory Appl., 26, pp.65-79, 1998.

EFFECTS OF TIMING JITTER IN TH-BPSK UWB SYSTEMS APPLYING THE FCC-CONSTRAINT PULSES UNDER NAKAGAMI-M FADING CHANNEL

Kwang Park, Jeungmin Joo
Department of Information and Communications, Republic of Korea
pk94@kjist.ac.kr

Sungsoo Choi, Kiseon Kim
Korea Electrotechnology Research Institude, Republic of Korea
sschoi@ieee.org

DOI: 10.36724/2664-066X-2021-7-6-21-25

ABSTRACT

Ultra wideband (UWB) technology has obtained lots of attention as a strong candidate for short range indoor wireless communication because of low power consumption, low cost implementation and the robustness against multipath fading. It uses trains of short pulses which widely spread the signal energy in frequency domain. Since such large bandwidth can cause interference with other narrow band communication systems, the federal communications commission (FCC) has restricted not only the frequency region from 3.1GHz to 10.6GHz but also the transmission power level for commercial use of UWB systems. The effects of timing jitter on time hopping binary phase shift keying (TH-BPSK) UWB systems applying the FCC-constraint pulses are investigated under flat Nakagami-mfading channel and additive white Gaussian noise (AWGN). The numerical results show that two FCC-constraint pulses, PSP and MMNHP, have almost same sensitivity to the timing jitter even though they have different transceiver complexity. Additionally, the additional required power due to the timing jitter exponentially increases, but that due to the amplitude fading is not exceeded over 4dB.

KEYWORDS: *Ultra wideband, communication systems, digital communication, Prolate Spheroidal Pulse.*

The article is reworked from unpublished 2nd IEEE International Conference on Circuits and Systems for Communications (ICCSC) materials.

Introduction

Ultra wideband (UWB) technology has obtained lots of attention as a strong candidate for short range indoor wireless communication because of low power consumption, low cost implementation and the robustness against multipath fading. It uses trains of short pulses which widely spread the signal energy in frequency domain. Since such large bandwidth can cause interference with other narrow band communication systems, the federal communications commission (FCC) has restricted not only the frequency region from 3.1GHz to 10.6GHz but also the transmission power level for commercial use of UWB systems in 2002 [1].

Typically, the Gaussian pulse has been considered in UWB communications [2],[3]. However, the Gaussian pulse itself does not give a good solution to satisfy the FCC regulations and must be modified [4],[5]. Therefore, UWB pulses need to be designed to satisfy the FCC regulations. Recently, UWB pulse design methods have been suggested for not only satisfying the FCC regulations but also generating multiple orthogonal pulses. Among them, modulated and modified hermite orthogonal pulse (MMNHP) uses carrier modulation method to meet the FCC regulations. Unlike MMNHP, prolate spheroidal pulse (PSP), which is based on prolate spheroidal wave function idea in the pulse design algorithm, employs the filtering method instead of using carrier. Even though both pulse generation methods employ the different pulse design method, they give advantages to generate multiple orthogonal pulses which can provide many advantages in multiple access environment [4],[6].

As a data modulation format, pulse position modulation (PPM) has been widely used in time hopping (TH) UWB systems due to the easy implementation. Recently, binary phase shift keying (BPSK) modulation is also being employed because of the advanced Complementary Metal Oxide Semiconductor (CMOS) and Silicon-Germanium (SiGe) technologies and advantages of high data rate and power efficiency over PPM [7].

Like any other digital communication, TH-BPSK UWB systems suffer from the timing jitter caused by imprecise clock generators. Hence, it is necessary to examine how much the timing jitter affects to the system performance according to UWB pulses. Consequently, we investigate the effects of the timing jitter on the full band (FB)-PSP and FB-MMNHP in TH-BPSK UWB systems and compare two pulses under the given timing jitter.

This paper is organized as follows : Section 2 reviews the conventional Gaussian pulse, MMNHP and PSP. In Section 3, TH-BPSK UWB signal model is described and the bit error rate (BER) of TH-BPSK UWB with the timing jitter in the presence of Nakagami-m fading channel is obtained in Section 4. Subsequently, the numerical results are shown in Section 5, and conclusions are given in Section 6.

UWB Pulses

The Gaussian pulse is given by

$$w_g(t) = 2\alpha\sqrt{e}\frac{t}{\tau_g}e^{-2(\frac{t}{\tau_g})^2} \tag{1}$$

where α denotes the peak amplitude of the pulse, τ_g is the pulse width adjustment parameter, and $\int_{-\infty}^{\infty} w_g(t)dt$ =0 is satisfied. By adjusting the parameter τ_g, the bandwidth of the Gaussian pulse is more widely spread up to 10.6GHz. However, there still remains co-interference problem with narrow band systems such as global positioning system (GPS) band (0.95GHz∼1.61GHz) and it violates FCC regulations. Thus, GP must be modified or filtered for satisfying the FCC rules [4],[5].

B. Modulated and Modifie Normalized Hermite Pulse (MMNHP)

MMNHP was proposed in [6]. This pulse is defined as

$$w_m(t) = \frac{1}{\sqrt{n!\sqrt{\pi/2}}}h_n(t)\sin(2\pi f_c t + \phi_r) \tag{2}$$

where $1/\sqrt{n!\sqrt{\pi/2}}$ is a normalization factor to obtain the unit energy, $h_n(t)$ is the modifie Hermite polynomial to obtain orthogonality property, which is represented by

$$\begin{aligned} h_n(t) &= \exp\left(-\frac{t^2}{4}\right)h_{e_n}(t) \\ &= (-1)^n \exp\left(\frac{t^2}{4}\right)\frac{d^n}{dt^n}\left(\exp\left(\frac{t^2}{2}\right)\right) \end{aligned} \tag{3}$$

PSD of MMNHP

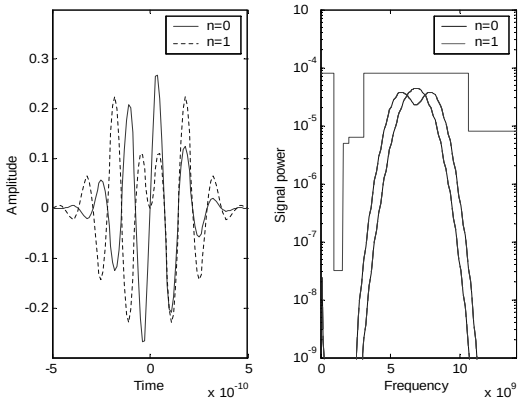

Fig. 1. 0th and 1st order MMNHP shapes and its power spectral density

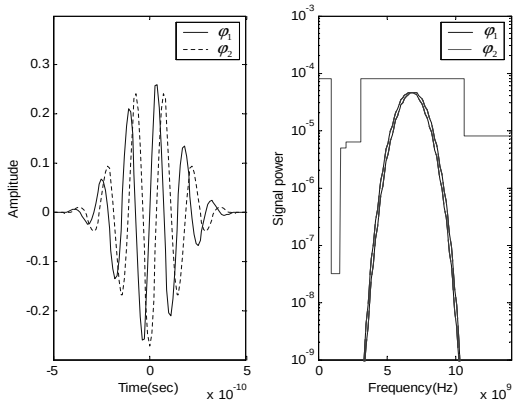

Fig. 2. PSP shapes w_{p_1} w_{p_2} and its power spectral density

where $h_{e_n}(t)$ is the original Hermite polynomial function. To meet the FCC requirement in frequency domain, a certain sinusoid function $sin(2\pi f_c t + \phi_r)$ should be multiplied to modifie normalized hermite pulse (MNHP), $h_n(t)$, where the center frequency f_c=6.85GHz is used. MMNHP and its power spectral density are plotted in Fig.1.

C. Prolate Spheroidal Pulse (PSP)

PSP is based on prolate spheroidal wave function idea in pulse design algorithm [4] and has many advantages over the Gaussian monocycle pulse. Basic idea of this algorithm is to use the impulse response $h(t)$ of the desired frequency mask $H(f)$ ($H(f) = 1, 3.1GHz < f < 10.6GHz$). When PSP, $w_p(t)$, passes through the filte $h(t)$, the filte output can be represented as a convolution form of $w_p(t)$ and $h(t)$, which is given by

$$\lambda w_p(t) = \int_{-T_m/2}^{T_m/2} w_p(\tau) h(t-\tau) d\tau, \tag{4}$$

where T_m is the pulse period and λ is the attenuation factor. By sampling at a rate of N samples per T_m, (4) is simplifie as follows:

$$\lambda w_p[n] = \sum_{m=-N/2}^{N/2} w_p[n] h[n-m], n = -\frac{N}{2} \cdots, \frac{N}{2} \tag{5}$$

(5) can also be expressed in vector form, which gives the simple solution to obtain the $w_p[n]$. When we choose $N = 100$ onal pulses. Two pulses w_{p_1}, w_{p_2} out of 101 pulses from the algorithm and their power spectral densities are plotted in Fig.2.

Signal Model

A TH signal using BPSK modulation from the kth user, $s^{(k)}(t)$, is given by

$$s^{(k)}(t) = \sum_{j=-\infty}^{\infty} (2d^{(k)}_{[j/N_s]} - 1) w(t - jT_f - c_j^{(k)} T_c - \varepsilon^{(k)}) \tag{6}$$

where $w(t)$ is the short duration pulse waveform, T_f is the frame time which is typically quite larger than the pulse width, $c_j^{(k)}$ is a pseudo-random code of the kth user, $c_j^{(k)} T_c$ represents the total time-hopping shift which is equal and less than T_f, and N_s is the number of pulse repetition per symbol, $d^{(k)}_{[j/N_s]}$ is the information sequence of kth user, the notation $[a]$ means the integer part of a and $\varepsilon^{(k)}$ is the timing jitter of the kth user.

Under the single user environment, the received signal $r(t)$ is represented as

$$r(t) = \alpha\, s(t) + n(t) \tag{7}$$

where α is the fading amplitude and $n(t)$ is the additive white Gaussian noise.

Numerical Analysis

To evaluate the effect of the timing jitter under Nakagami-m fading channel, we assume that the fading is slow that the channel coherence time is larger than the symbol time duration. Therefore, the conditional error probability of TH-BPSK UWB system with the timing jitter is represented as

$$P_b(E|\varepsilon, \alpha) = Q\left(\sqrt{\frac{(\alpha N_s m_p)^2}{\sigma^2_{rec}}}\right) \tag{8}$$

where α is the fading amplitude, which is a random variable with $\alpha^2 = \Omega$ and probability density function (pdf) of α is the

Nakagami-m distributed, N_s is the number of the pulse repetition, and m_p is the autocorrelation function of $w(t)$, which is represented as

$$_p = \int_{-\infty}^{\infty} w(t-\varepsilon) w(t) dt = R_w(\varepsilon) \tag{9}$$

When ε is zero, $R_w(0)$ is equal to the pulse energy $E_p = \int_{-\infty}^{\infty} w^2(t) dt$ and σ^2_{rec} is given by

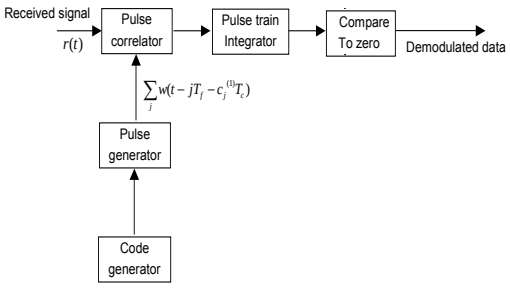

Fig. 3. Receiver Structure for TH-BPSK UWB System

$$\begin{aligned}\sigma_{rec}^2 &= E\left([\int n(t)w_{bit}(t)dt]^2\right) \\ &= \frac{N_o}{2}\int_{-\infty}^{\infty} w_{bit}^2(t)dt \end{aligned} \quad (10)$$

where $w_{bit}(t) = \sum_{j=iN_s}^{(i+1)N_s-1} w(t - jT_f - c_j^{(k)}T_c)$ and σ_{rec}^2 is represented as

$$\sigma_{rec}^2 = \frac{N_o N_s E_p}{2} \quad (11)$$

Consequently, the conditional error probability of TH-BPSK UWB system with the timing jitter is represented as

$$P_b(E|\varepsilon,\alpha) = Q\left(\sqrt{\frac{2\alpha^2 N_s^2 R_w^2(\varepsilon)}{N_o E_p}}\right) \quad (12)$$

The error probability is obtained by averaging (12) over the pdf of the timing jitter ε and the pdf of the instantaneous pulse-signal-to-noise power ratio (PSNR) $\gamma = \frac{\alpha^2 E_p}{N_o}$, it is represented as

$$P_b(E) = \int_{-\varepsilon_m}^{\varepsilon_m}\int_0^{\infty} Q\left(\sqrt{2N_s\gamma A^2(\varepsilon)}\right) f_\gamma(\gamma) f_\varepsilon(\varepsilon)d\gamma d\varepsilon \quad (13)$$

where we let $A(\varepsilon) = \frac{R_w(\varepsilon)}{E_p}$, which is the only dependent value on ε, not γ. And $f_\gamma(\gamma)$ is the Gamma distribution which is represented as

$$f_\gamma(\gamma) = \frac{m^m \gamma^{m-1}}{\overline{\gamma}^m \Gamma(m)} \exp(-\frac{m\gamma}{\overline{\gamma}}) \quad (14)$$

where $\overline{\gamma} = \frac{\overline{\alpha}^2 E_p}{N_o}$ is the average PSNR, and $f(\varepsilon)$ is the pdf of the timing jitter, which is assumed to be uniformly distributed

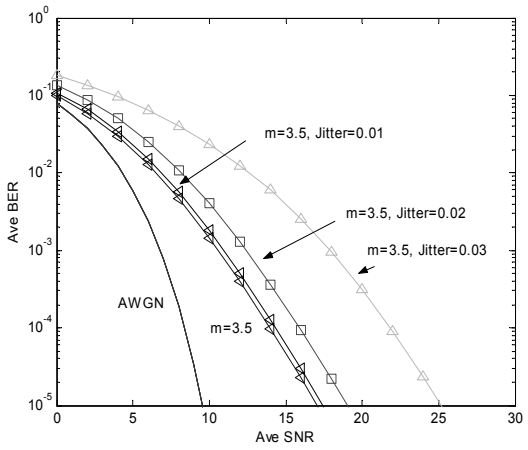

Fig. 4. Average BER of TH-BPSK using FB-PSP under fla Nakagami-m fading channel, for $N_s = 24$

in the range of $[-\varepsilon_{max}, \varepsilon_{max}]$. Using an alternative Gaussian expression [9], the average error probability is represented as follows

$$P_b(E) = \frac{1}{2\pi\varepsilon_{max}}\int_{-\varepsilon_{max}}^{\varepsilon_{max}}\int_0^{\frac{\pi}{2}} \left(1 + \frac{N_s\overline{\gamma}A(\varepsilon)^2}{m\sin^2\theta}\right)^{-m} d\theta d\varepsilon \quad (15)$$

According to the measurement data [10], the parameter m is truncated Gaussian random variables with mean μ_m=3.5, where fi ed mean μ_m=3.5 value is simply chosen for numerical evaluation in this paper.

Numerical Results

To investigate the sensitivity to the timing jitter on the FB-PSP, the pulse is normalized to the unit energy. Time duration T_c is set to $1ns$ for all pulses, and the timing jitter is assumed to be uniformly distributed in the range of $[-\varepsilon_{max}, \varepsilon_{max}]$, where the normalized timing jitter factor is define as ε_{max}/T_c. ($\varepsilon_{max}/T_c \leq 1$).

In Figure 4, the sensitivity of the BER for the FB-PSP due to the timing jitter is depicted for $\varepsilon_{max} = 0.01ns$, $0.02ns$ and $0.03ns$, respectively. For satisfying the BER performance of 10^{-3}, the SNR of 6.77dB is required in no timing jitter case under AWGN, whereas the additional power of 3.8dB is required under fla Nakagami-m fading channel with fi ed m=3.5, and the additional power of more than 11.16dB is required in $\varepsilon_{max} = 0.03ns$ case under Nakagami-m fading channel.

In Figure 5, when the timing jitter changes, the additional required power for getting the BER of 10^{-3} is described under flat Nakagami-m fading channel and AWGN for N_s=24, respectively. As shown in the figure, the additional required power increases exponentially as the timing jitter increases under both Nakagami-m fading channel and AWGN.

For in-stance, the additional power of 4.16dB is required with the timing jitter of $0.01ns$, whereas the additional power of about 11dB is required with the timing jitter of $0.03ns$ under flat Nakagami-m fading channel. Additionally, the additional power caused by the amplitude fading slightly decreases as the timing jitter decreases.

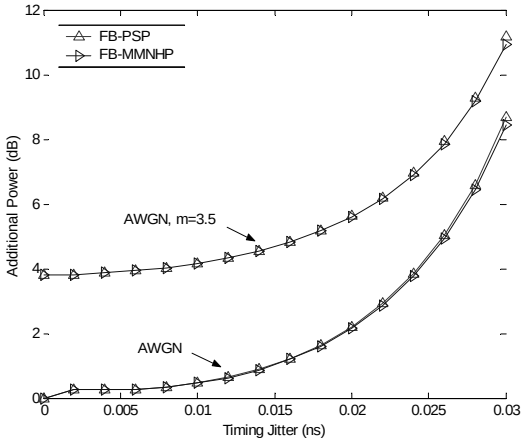

Fig. 5. Additional power as a function of the timing jitter under flat Nakagami-m fading channel and AWGN, for satisfying $P_e = 10^{-3}$

In Figure 6, the additional required power caused by the fad-ing effect and the timing jitter for getting 10^{-3} is described for N_s=24, respectively. The additional required power caused by the timing jitter increases exponentially under AWGN, whereas the fading effect slightly decreases as the timing jit-ter increases. Thereby two curves meet at the certain point, the timing jitter=$0.0277ns$. It is concluded that the timing jit-ter of more than $0.0277ns$ is more dominant factor to affect the system performance than the fading effect.

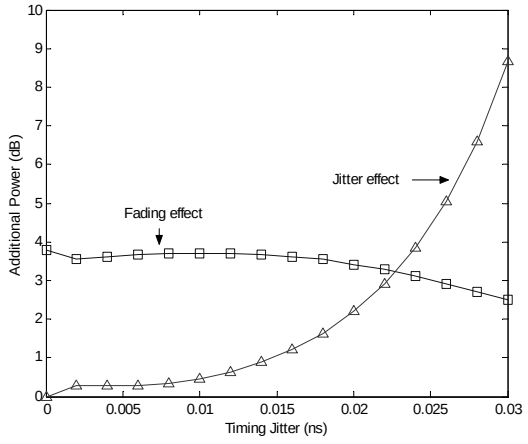

Fig. 6. Additional power as a function of the timing jitter under flat Nakagami-m fading channel and AWGN, for satisfying $P_e = 10^{-3}$

And it is notable that the degradation caused by the timing jitter is not simply compensated by increasing the number of pulse repetition under single user case. Therefore, more precise tracking devices should be required to compensate the degradation caused by the timing jitter.

Considering the transmitter complexity, to generate the conventional Gaussian pulse is relatively easier than to generate both PSP and MMNHP. However, the Gaussian pulse itself does not give a good solution to meet the FCC rules and should be modified or filtered because the Gaussian pulse violates FCC regulations. For MMNHP generation, an additional sinusoid multiplier is required to meet the FCC regulations, whereas no multiplier is required for the PSP generation which use the filtering method instead.

Conclusions

In this paper, with the FCC-constraint pulses (FB-PSP, FB-MMNHP), effects of timing jitter on the FB-PSP are investigated and compared with FB-MMNHP in TH-BPSK UWB systems in the presence of flat Nakagami-m fading channel and AWGN. It is shown that two FCC-constraint pulses, FB-PSP and FB-MMNHP, have almost same sensitivity to the timing jitter even though they have different complexity. And the results show that degradation caused by the amplitude fading is more dominant factor to affect the system performance than that caused by the timing jitter in the range of less than $0.0277ns$. The timing jitter increases exponentially unlike the amplitude fading effect. Therefore, precise tracking devices are required when the FCC-constraint pulses are applied.

References

[1] G.R. Aiello and G.D. Rogerson, "Ultra-Wideband Wireless Systems," *IEEE microwave magazine,03*, pp. 36-47, June 2003.

[2] R.A. Scholtz, "Multiple Access with Time Hopping Impulse Modulation," *Proc.IEEE MILCOM,93*, vol. 2, pp.447-450, Oct 1993.

[3] W.M. Lovelace and J.K. Townsend, "The Effects of Timing Jitter and Tracking on the Performance of Impulse Radio," *IEEE JSAC,02*, vol. 20, no. 9, pp.1646-1651, Dec 2002.

[4] B. Parr, B.L. Cho, and K. Wallace, "A Novel Ultra-Wideband Pulse Design Algorithm"," *IEEE communication letters*, vol. 7, no. 5, pp.219-221, May 2003.

[5] X. Luo, L. Yang and G.B. Giannakis, "Designing Optimal Pulse-Shapers for Ultra-Wideband Radios," *JCN*, vol. 5, no. 4, pp.344-353, Dec 2003.

[6] M. Ghavami, L.B. Michael and R. Kohno, " Hermite Function Based Orthogonal Pulses for Ultra Wideband Communications," *In WPMC, 2001*, pp.42-46, May 2001.

[7] http://www.xtremespectrum.com.

[8] K. Park, J.M. Joo, H.K. Lee and K.S. Kim, "Effects of Timing Jittr on Prolate Speroidal Pulse in Multiple Access Time-Hopping BPSK UWB Systems," To be accepted in ITC-CSCC, 2004.

[9] J.W. Graig, "A new, simple and exact result for calculating the probability of error for two-dimensional signal constellations," *IEEE MILCOM,91*, vol. 2, pp.571-575, Nov. 1991.

[10] D. Cassioli, M.Z. Win and A.F. Molisch, "The Ultra-Wide Bandwidth Indoor Channel: From Statistical Model to Simulations," *IEEE JSAC,02*, vol. 20, no. 6, pp.1247-1257, Aug 2002.

[11] M.K. Simon and M.S. Alouini, "Digital communications over fading channels : a unified approach to performance analysis," *John Wiley and Sons*, New York, 2000.

ENHANCED V-BLAST PERFORMANCE IN MIMO WIRELESS COMMUNICATION SYSTEMS

Byung Moo Lee, Rui J. P. de Figueiredo
Laboratory for Intelligent Signal Processing and Communications University of California, Irvine
byungl@uci.edu, rui@uci.edu

DOI: 10.36724/2664-066X-2021-7-6-26-30

ABSTRACT

We have presented performance analysis of E-V-BLAST and according to this analysis, we found some useful characteristics of the E-V-BLAST algorithm for performance and complexity trade-off. Increasing S is applying ML detection with depth T for some most error likely signals. Increasing T is improving the ML detection with depth T . Increasing T will not affect so much to the performance of E-V-BLAST at high SNR. The importance of increasing T depends on S. Recently, a new detection algorithm for the Verti- cal Bell Laboratories Layered Space Time (V-BLAST) system, which we call Enhanced-V-BLAST, or simply E-V-BLAST, was proposed. In the present paper, we analyze the performance of E- V-BLAST as a function of the two inherent adjustable parameters of E-V-BLAST. On the basis of this analysis, we obtain some useful characteristics of the E-V-BLAST algorithm which allow one to achieve the desired performance and complexity trade-off.

KEYWORDS: *Vertical Bell Laboratories Layered Space Time, Wireless Communication Systems, MIMO.*

The article is reworked from unpublished 2nd IEEE International Conference on Circuits and Systems for Communications (ICCSC) materials.

The Vertical Bell Laboratories Layered Space Time (V-BLAST) system is a powerful detection algorithm for band-width efficient multiple antenna wireless communication sys-tem [2], [3], [4]. Although, V-BLAST has demonstrated very high spectral efficiency, there is a wide gap between the orig-inal V-BLAST algorithm and the Maximum Likelihood (ML) algorithm. Recently, some algorithms have been presented to make narrower this gap [1], [5], [7], [8], [9], [10]. In [1], a new detection algorithm (Enhanced (E) -V BLAST) for V-BLAST system was presented which showed significantly better performance and flexibility than the original V-BLAST detection. The E-V-BLAST algorithm gets closer to the op-timum detection Maximum Likelihood (ML) algorithm by making decisions based on multiple symbols. The Enhanced (E) -V-BLAST has two parameters which can be adjusted to achieve a desired performance and complexity trade-off. The main idea in E-V-BLAST is that, instead of making an immediate decision on a symbol being detected and cancelled at an iteration step, the decision about that symbol is made at a later level based on the multiple symbol possibilities that have accumulated by descending a tree of width S and depth T.

In what follows, we provide an analysis of the E-V-BLAST system. We analyze the performance of E-V-BLAST and compare the cases of various parameters which we can adjust for performance and complexity trade-off.

The remaining sections are organized as follows. In section II, we address the system model and overview original V-BLAST algorithm. In section III, we present E-V-BLAST algorithm which was introduced recently and analyze its performance. Some simulation studies are shown in section IV. We end in section V by presenting some conclusions.

SYSTEM MODEL

Let M denote the number of transmitting antennas and let N denote the number of receiving antennas in the wireless mul-tiple antenna communication system. The (M, N) single user system under consideration is depicted in Figure 1.

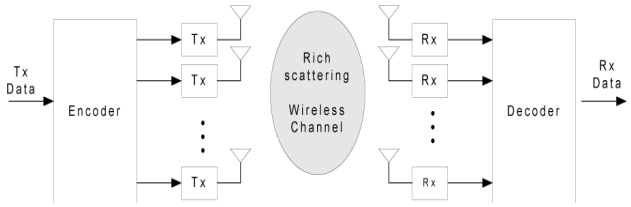

Fig. 1. Block diagram of V-BLAST system

Throughout this paper, we assume N = M for simplicity. It is assumed that there are considerable scattering takes place in the environment and that all the antennas are spaced for uncorrelated fading. We assume perfect channel state information at the receiver. The source stream is demultiplexed into M substreams, each transmitted from an antenna independently and simultaneously. The received signal r in complex baseband representation can be written as

$$r = Ha + \nu \quad (1)$$

where ν is a complex Gaussian noise vector with zero mean and variance σ^2_ν, a is transmitted signal vector and H is an $N \times M$ channel matrix whose elements are i.i.d complex Gaussian random variables with zero mean and unit variance.

ENHANCED V-BLAST ALGORITHM

The original V-BLAST embodies the simplest possible solutions. The Enhanced V-BLAST or simply E-V-BLAST algorithm gets closer to optimum detection by making decisions based on multiple symbols. In this section, we review the E-V-BLAST algorithm and conduct an approximate performance analysis. The idea of E-V-BLAST algorithm can be applied to any detection algorithm, detection using Pseudo inverse or QR decomposition. In this paper, we use Pseudo inverse detection for the explanation of E-V-BLAST.

A. E-V-BLAST algorithm

Optimum detection or Maximum Likelihood (ML) detection is computationally very expensive. So, in E-V-BLAST algorithm, we do the following two things.

1. In ead of ML detection of the signal based on all M, we make a symbol decision based on T (where $T \leq M$), and continue iteratively.

2. Instead of considering all the possible symbols of our constellation, we consider only the S best (nearest neighbors) symbols.

These two variables, S and T, are adjustable parameters of the algorithm. Their highest possible values are the total number of transmitters for T and the constellation size for S. In this case, detection will correspond to the ML case and will therefore have the highest possible computational complexity. In the simplest case (when $T = 1$, $S = 1$), the algorithm will be equivalent to original V-BLAST. When a decision is made, the best paths are kept and the rest are discarded.

The E-V-BLAST algorithm is explained with an example in Table 1 where we have initially assumed $T = 2$ and $S = 2$. By choosing $T = 2$ we delay every decision until the following recursion. The choice of S implies that decisions are made based on the combined distance of 2 different transmitter symbols. The two nearest symbols are chosen as shown in Figure 2. We call this operation "Multiple Slicing" and write it as $Q(y_1) = (a_{1,1}, a_{1,2})$, where $Q(y_1)$ denotes the slicing operation resulting in potential candidates $(a_{1,1}, a_{1,2})$. E-V-BLAST also use optimal ordering and DFE like conventional V-BLAST. To completely understand the algorithm, Table 1 should be followed.

Table 1

Example of detection with E-V-BLAST algorithm, S = 2, T = 2 [1]

Column 1	Column 2	Column 3
$r_1 = z_{1,1}a_1 + \nu_1$ • Form 2 potential candidates symbols (2 nearest neighbors) • Find distance metrics corresponding to each symbol • Find updated received vectors due to each, using symbol cancellation.	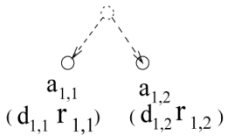	$y_1 = \mathbf{w}_1^T \mathbf{r}$ $(a_{1,1}, a_{1,2}) = Q(y_1)$ $d_{1,1} = \frac{\lvert y_1 - a_{1,1}\rvert^2}{\lVert \mathbf{w}_1^T \rVert^2}$ $d_{1,2} = \frac{\lvert y_1 - a_{1,2}\rvert^2}{\lVert \mathbf{w}_1^T \rVert^2}$ $\mathbf{r}_{1,1} = \mathbf{r} - a_{1,1}(\mathbf{H})_1$ $\mathbf{r}_{1,2} = \mathbf{r} - a_{1,2}(\mathbf{H})_1$
$r_2 = z_{2,1}\hat{a}_1 + z_{2,2}a_2 + \nu_2$ • Form total 4 potential candidates. Two assuming $a_1 = a_{1,1}$ and two assuming $a_1 = a_{1,2}$ • Find distance metrics for each new potential candidate. Parent node distances are incorporated in the child node distances. These distances are used for decision and pruning of tree. • Form updated received vectors due to each new statistic, using symbol cancellation. • Decision: Find node corresponding to minimum distance (say $a_{2,3}$). Parent of this node ($a_{1,2}$) is the final detected symbol for previous level (transmitter) • Discard undetected parent($a_{1,1}$) and its children	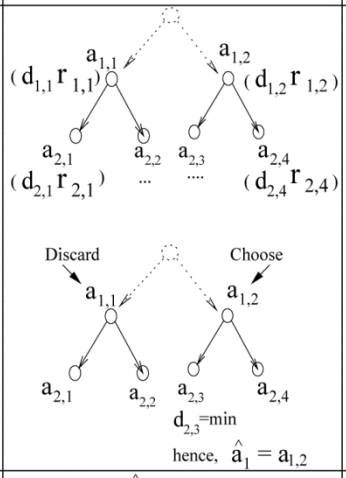	$y_{11} = \mathbf{w}_2^T \mathbf{r}_{1,1}$ $(a_{2,1}, a_{2,2}) = Q(y_{11})$ $d_{2,1} = \frac{\lvert y_1 - a_{1,1}\rvert^2}{\lVert \mathbf{w}_1^T \rVert^2} + \frac{\lvert y_{11} - a_{2,1}\rvert^2}{\lVert \mathbf{w}_2^T \rVert^2}$ $= d_{1,1} + \frac{\lvert y_{11} - a_{2,1}\rvert^2}{\lVert \mathbf{w}_2^T \rVert^2}$ $d_{2,2} = d_{1,1} + \frac{\lvert y_{11} - a_{2,2}\rvert^2}{\lVert \mathbf{w}_2^T \rVert^2}$ $\mathbf{r}_{2,1} = \mathbf{r}_{1,1} - a_{2,1}(\mathbf{H})_2$ $\mathbf{r}_{2,2} = \mathbf{r}_{1,1} - a_{2,2}(\mathbf{H})_2$ $y_{12} = \mathbf{w}_2^T \mathbf{r}_{1,2}$ etc. Similarly find $a_{2,3}, d_{2,3}, \mathbf{r}_{23}, a_{2,4}$ etc. if minimum distance $= d_{2,3}$ choose $\hat{a_1} = a_{1,2}$
$r_3 = z_{3,1}\hat{a}_1 + z_{3,2}\hat{a}_2 + z_{3,3}a_3 + \nu_2$ • After pruning, we have two potential candidates remaining for previous level. • Similar situation as in the beginning of row 2 above. • Rename, and continue recursively to detect all transmitter symbols.	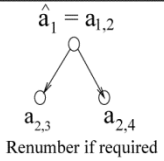	Continue recursively, repeat steps above for new tentative symbols. Last symbol remaining at the end is detected based on its minimum distance.

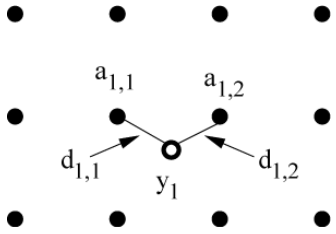

Fig. 2. Multiple Slicing: Choosing two possible candidates for a statistic

B. Approximate Performance Analysis of E-V-BLAST

In this subsection, we approximately analyze the performance of E-V-BLAST system. As we can see in the results of [5], all of signal errors are limited by the worst subchannel or performance of the first signal detection.

$$P[E_j] \leqslant P[E_1] \cdot \frac{1}{1-\epsilon}, \quad j = 2, 3, \cdots, M \tag{2}$$

where $\in$ is very small positive number for large SNR. This is because of inherent error propagation of Decision Feedback Equalization (DFE) in V-BLAST detection. Any detection error in the first signal will most likely result in detection errors of next signals. If we use feedforward matrix Q^H, the Hermitian of Q matrix after QR factorization, the elements of channel matrix will have different degree of freedom [5]. If we use pseudo inverse w^T_i, the post-detection SNR is changed [4]

$$SNR_i = \frac{< |a_i|^2 >}{\sigma_\nu^2 \|\mathbf{w}_i\|^2} \tag{3}$$

We carry out performance analysis of the first signal with i.i.d. Rayleigh fading channel and Additive White Gaussian Noise (AWGN). We use ZF (Zero Forcing)-V-BLAST, so we can regard all of interference is zero, when we detect the first signal of E-V-BLAST.

We define metric as

$$m(r_j, a_j; z_{j,j}) = -|r_j - z_{j,j}\, a_j|^2 \tag{4}$$

where $z_{j,j}$ is channel matrix component after ZF. We will use Pairwise Error probability (PEP) and union bound for analysis of performance. PEP is defined to be the probability of choosing the nearest signal of a_i, namely, $\hat{a}_i$, when a_i was transmitted. With perfect channel state information (CSI), PEP can be represented as

$$P_2(a_1 \to \hat{a}_1|z_{1,1}) = P[m(r_1, \hat{a}_1; z_{1,1}) \geq m(r_1, a_1; z_{1,1})] \tag{5}$$

If we use Chernoff bound for Q function

$$\begin{aligned} P_2(a_1 \to \hat{a}_1|z_{1,1}) &= Q\left(\sqrt{\frac{d_{min}^2 z_{1,1}^2}{4\sigma_\nu^2}}\right) \\ &\leq exp\left(-\frac{d_{min}^2 z_{1,1}^2}{8\sigma_\nu^2}\right) \end{aligned} \tag{6}$$

Where $d_{\min}^2 = |a_1 - \hat{a}_1|^2$. Averaging (6) with respect to $z_{1,1}$ yields

$$\begin{aligned} P_2(a_1 \to \hat{a}_1) &\leq E_{z_{1,1}}\left[exp\left(-\frac{d_{min}^2 z_{1,1}^2}{8\sigma_\nu^2}\right)\right] \\ &= \frac{1}{\left(1 + \frac{d_{min}^2}{4\sigma_\nu^2}\right)} \end{aligned} \tag{7}$$

When applying union bound, we should separate error bound in two parts. One part is normal detection and the other part is the effect of E-V-BLAST algorithm.

$$\begin{aligned} P(E_1) &\leq \frac{M_c - S}{\left(1 + \frac{d_{min}^2}{4\sigma_\nu^2}\right)} \\ &+ S \cdot P[m_T(\acute{\mathbf{r}}, \hat{\mathbf{a}}; \acute{\mathbf{Z}}) \geq m_T(\acute{\mathbf{r}}, \mathbf{a}; \acute{\mathbf{Z}})] \end{aligned} \tag{8}$$

where M_c is signal constellation size and $m_T(\acute{\mathbf{r}}, \mathbf{a}; \acute{\mathbf{Z}}) = -\sum_{j=1}^{T} |\acute{r}_j - \sum_{i=1}^{T} \acute{z}_{j,i} a_i|^2$

r_j' is assumed the received signal after relevant Zero Forcing(ZF) operation for performing ML detection with depth T . One of example of this kind of operation can be found in [5]. More specifically, when T = 2, we can represent Z´ as

$$\acute{\mathbf{Z}} = \begin{pmatrix} \acute{z}_{1,1} & \acute{z}_{1,2} & 0 & 0 & \dots & 0 \\ \acute{z}_{2,1} & \acute{z}_{2,2} & 0 & 0 & \dots & \vdots \\ \acute{z}_{3,1} & \acute{z}_{3,2} & \acute{z}_{3,3} & 0 & \dots & \vdots \\ \vdots & \vdots & \vdots & \ddots & \ddots & 0 \\ \acute{z}_{M,1} & \dots & \dots & \dots & \acute{z}_{M,M-1} & \acute{z}_{M,M} \end{pmatrix} \tag{9}$$

Equation (8) will be clear, if we think about the algorithm.

We choose *S* signals and delay the decision of these signals in depth *T*. This means we choose some most error-prone signals *S* and apply modified ML detection with depth *T* for the error-prone signals.

The second part of (8) can be

$$\begin{aligned} & P \quad [m_T(\acute{\mathbf{r}}, \hat{\mathbf{a}}; \acute{\mathbf{Z}}) \geq m_T(\acute{\mathbf{r}}, \mathbf{a}; \acute{\mathbf{Z}})] \\ & \leq \quad E_{\acute{\mathbf{Z}}}\left(\prod_{j=1}^{T} exp\left(-\frac{1}{8\sigma_\nu^2}\left|\sum_{i=1}^{T} \acute{z}_{j,i}(a_i - \hat{a}_i)\right|^2\right)\right) \\ & = \quad \frac{1}{\prod_{j=1}^{T}\left(1 + \frac{d_T^2}{4\sigma_\nu^2}\right)} \\ & = \quad \frac{1}{\left(1 + \frac{d_T^2}{4\sigma_\nu^2}\right)^T} \end{aligned}$$

where $d_T^2 = \sum_{i=1}^{T} |a_i - \hat{a}_i|^2$. (10)

Finally, we can express the error bound of E-V-BLAST as

$$P(E_1) \leq \frac{M_c - S}{\left(1 + \frac{d_{min}^2}{4\sigma_\nu^2}\right)} + \frac{S}{\left(1 + \frac{d_T^2}{4\sigma_\nu^2}\right)^T} \tag{11}$$

where $1 \leq S \leq M_c$ and $1 \leq T \leq M$. *S* and *T* are integers.

As we wrote above, the second part of (11) is a kind of ML detection. Therefore, basically what E-V-BLAST algorithm does is using modified ML detection or ML detection with depth *T* for some signal constellation which is most likely to be in error. According to the equation (11), we may ascertain some characteristics of E-V-BLAST. Increasing S means moving some of most error-prone signals in signal constellation from conventional V-BLAST detection to modified ML detection. Increasing *T* means improving the performance of modified ML detection part. Increasing *S* will show good performance at high SNR. But, the effect of increasing S will be reduced as *S* increased, because of signal constellation structure. The effect of increasing *T* will be reduced as SNR increases. Because at high SNR, the second term of equation (11) will be ignored, the error performance will be bounded at the first term of equation (11). As we can see, the first term of equation (11) is independent of *T*. So increasing *T* will not affect the error probability at high SNR. One more thing we should consider here is that in the highest complexity case ($S = M_c$, $T = M$), equation (11) becomes the usual ML detection.

SIMULATION RESULTS

The E-V-BLAST algorithm was tested by simulation using various *S* and *T* for a (5,5) uncoded system. Information symbols are modulated using 16QAM. According to the Figure 3, increasing *S* significantly improves the performance especially at high SNR. But, the effect of *S* is reduced as *S* is increased. This is because of signal constellation structure of QAM. Error usually occurs with right to the nearest neighbors. Increasing *S* covers the nearest neighbors step by step. So the effect of *S* is reduced as *S* is increased.

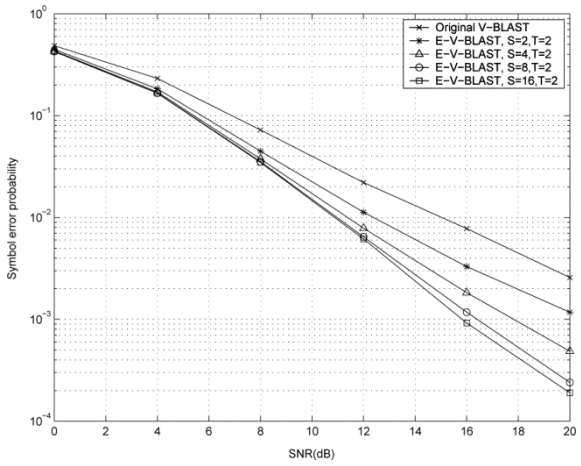

Fig. 3. Performance comparison of E-V-BLAST for increasing *S* and fixed *T*, uncoded (5, 5) 16 QAM

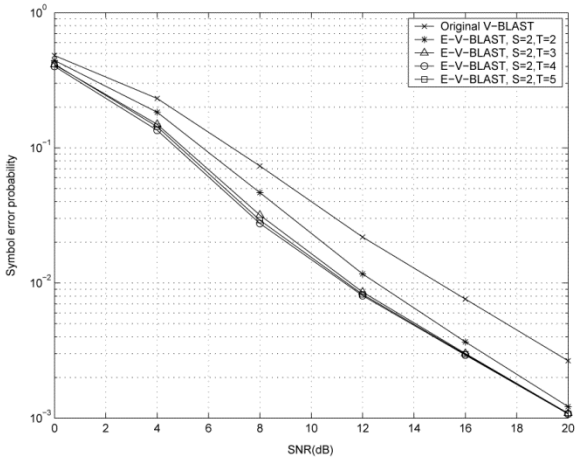

Fig. 4. Performance comparison of E-V-BLAST for increasing *T* and fixed *S*, uncoded (5, 5) 16 QAM

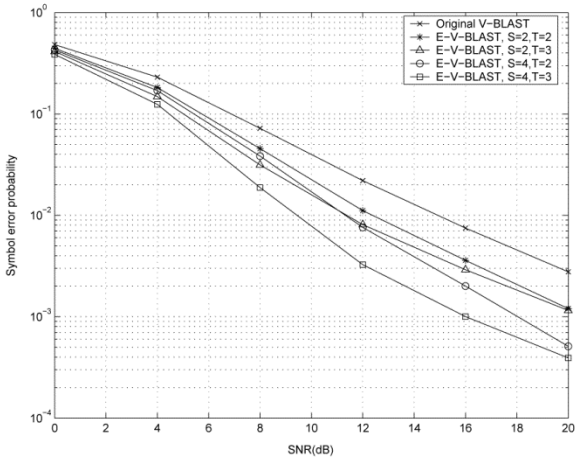

Fig. 5. Performance comparison of E-V-BLAST for increasing *T*, when *S* is changed, uncoded (5, 5) 16 QAM

Figure 4 shows at high SNR, the effect of *T* is not so significant. At high SNR, we can ignore the second term of (11), regardless of the value of *T*.

In this case, basically, the error probability (11) is bounded in the first term of (11). So all of the system performance of increasing *T*, but fixed *S* system will be same at the high SNR. The simulation of Figure 4 is the case of $S = 2$. If *S* is higher, then the effect of T will be increased, However, as shown in Figure 5, eventually, it also shows same behavior as mentioned above. These results induce us how we can reduce error probability efficiently.

CONCLUSION

We have presented performance analysis of E-V-BLAST and according to this analysis, we found some useful characteristics of the E-V-BLAST algorithm for performance and complexity trade-off. Increasing *S* is applying ML detection with depth *T* for some most error likely signals. Increasing *T* is improving the ML detection with depth *T*. Increasing T will not affect so much to the performance of E-V-BLAST at high SNR. The importance of increasing *T* depends on *S*. That is, the importance of increasing *T* depends on how many signals will be used for ML detection with depth *T*. Based on the analysis shown in this paper, we can use relevant level of *S* and *T*, depending on circumstances.

REFERENCES

[1] Ashish Bhargave, Rui. J. P. de Figueiredo and Torbjorn Eltoft. A Detection algorithm for the V-BLAST System,. *GLOBECOM 01, IEEE 2001*, Vol 1 pp. 494-498.

[2] G.J. Foschini. Layered Space-Time Architecture for Wireless Communication in a Fading Environment When Using Multiple Antennas, *Bell Laboratories Technical Journal*, Vol. 1,No 2, pp. 41-59, Autumn 1996.

[3] G.J. Foschini and M.J. Gans. On the Limits of Wireless Communication in a Fading Environment When Using Multiple Antennas, *Wireless Personal Communications*, Vol. 6(3), pp. 311-335, 1998.

[4] P.W. Wolniansky, G.J. Foschini, G.D. Golden, R.A. Valenzuela. V-BLAST: An architecture for realizing very high data-rates over the rich-scattering wireless channel, *Proc. IEEE ISSSE-98*, Pisa, Italy, 30th September 1998. IEEE.

[5] Won-Joon Choi, Rohit Negi, and John M. Cioffi. Combined ML and DFE decoding for the V-BLAST System, *Proc. IEEE ICC-00*, New Orleans, LA, USA, pp.18-22 June 2000.

[6] John G. Proakis, Digital Communications. *McGraw-Hill, third edition, 1995.*

[7] D. Wubben, R. Bohnke, J. Rinas, V. Kuhn, K.D. Kammeyer. Efficient algorithm for decoding layered space-time codes, *Electronics Letters*, Vol. 37, Issue 22, pp. 1348-1350, Oct. 2001.

[8] M.O. Damen, K. Abed-Meraim, and S. Burykh. Iterative QR detection for BLAST, *Wireless Personal Communications*, Vol 19, No 3, pp. 179-192, Dec. 2001.

[9] Ke Liu and Akbar M. Sayeed. An Iterative Extension of BLAST Decoding Algorithm for Layered Space-Time Signals, *Submitted to the IEEE Transactions on Communications*, Oct. 2002.

[10] M. Sellathurai and S. Haykin. Turbo-BLAST for Wireless Communications:Theory and Experiments, *IEEE Transactions on Signal Processing*, Vol. 50, pp. 2538-2546, Oct. 2002.

TOPICS IN COMMUNICATIONS WITH CHAOTIC SYSTEMS

Martin Hasler, Thomas Schimming
Laboratory of Nonlinear System, School of Computer and Communication Sciences Swiss Federal Institute of Technology Lausanne (EPFL) Lausanne, Switzerland

DOI: 10.36724/2664-066X-2021-7-6-31-35

ABSTRACT

The use of chaotic systems in communications approaches the threshold for industrial applicability. We shall give here an overview over a few techniques we think are promising. However, this overview does not pretend to be complete and it contains personal views on the subject. Also, the use of chaotic system for information encryption is not discussed at all. Only a choice of methods for coding and modulation for the transmission of digital information will be presented. An overview of a number of techniques to transmit information using chaotic systems is given. The difficulties in obtaining a good performance of such systems with respect to channel noise leads to fundamental question, to which we give a possible answer. Given the generally mediocre performance of such approaches, we have identified two fundamental questions which should help us pinpoint the main problems with the existing approaches with the help of information theory and communication theory. In particular it has been confirmed both in theory and by a constructive approach leading to a controlled variant of CSK, that indeed the information generated by free running chaotic systems (as captured by the Kolmogorov-Sinai entropy) is the problem, and the solution is a suitable control that makes this information part of the payload.

KEYWORDS: *Chaos, Communications, Noise performance, information theory, modulation, coding.*

The article is reworked from unpublished 2nd IEEE International Conference on Circuits and Systems for Communications (ICCSC) materials.

Introduction

The main features of chaotic systems that can be advantageously exploited for digital communications are

- Chaotic systems are simple to implement, at least at low frequencies [1]. Analog or mixed signal circuits can be used.
- Chaotic signals, i.e. signals produced by chaotic systems can be designed to have a smooth spectrum. The shape of the spectrum can be engineered [2, 3].

Direct chaotic communications

In direct chaotic communications [4], the chaotic signal that carries the information is directly sent over the communication channel. Since chaotic signals have a relatively wide spectrum, this method can only be applied in Ultra-Wideband communications. The basic block diagram of such a communication system is very simple (Fig. 1).

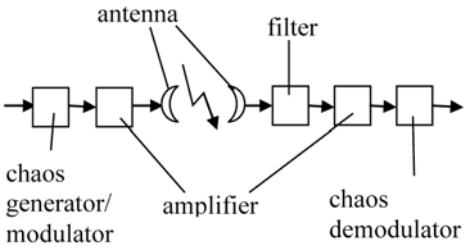

Fig. 1. Block diagram for direct chaotic communications

The advantage of this scheme is its simplicity and its low power consumption, by avoiding up- and down-modulation to base- or intermediate frequency bands. The difficulty lies in the realization of a chaos generator of sufficient quality. Related to this is the limitation to relatively simple modulation schemes, such as on-off keying. With respect to more conventional Ultra-Wideband communication schemes, its advantage lies in a smooth power spectrum of the emitted signal and thus lower peaks of its power spectrum for given total power.

Spreading codes using chaotic systems

In direct-sequence spread spectrum communications, for each bit that is to be transmitted, a rather long binary codeword is sent. For a whole message, the same codeword is used, multiplied either by 1 or by -1, depending on the value of the bit. This procedure increases the bandwidth of the transmitted signal. For this reason, the term spread spectrum is used and the codeword is called spreading sequence. The exaggerated use of frequency spectrum by a single user is compensated by letting several users with close to orthogonal spreading codes share the same frequency band.

Usually, special pseudorandom sequences, the Gold or M-codes, are used as spreading sequences. By using discrete-time chaotic systems whose output signal is 1-bit quantized, a large number of other pseudo-random codes can be generated. Usually, iterations of 1-dimensional maps are used to generate the spreading sequences. Careful optimization of the 1-dimensional maps allow to improve performance with respect to interference with other users of the same frequency band [5] (who use different spreading sequences), as well as multi-path interference performance [6].

In this application, no chaotic signal is sent over the communication channel, chaotic systems are only used to produce finite-length binary signals that have properties suitable for serving as spreading sequences in DS-CDMA systems. The merits and drawbacks of DS-CDMA systems are not any different than when conventional spreading sequences are used, except that more efficient spreading sequences can be produced. In addition, the number of good spreading sequences at the disposal of the system designer is increased considerably by using chaotic systems.

Chaos shift keying (CSK) And differential chaos shift keying (DCSK)

This techniques have been proposed already a decade ago [7, 8, 9, 10] and since then their performance with respect to additive white Gaussian noise in the channel (AWGN-channel) has been studied in depth [11, 12, 13].

This class of techniques mixes the information with a chaotic signal in the base-band or in an intermediate band, and then up-modulates them with a sinusoidal carrier signal. On the receiver side, the signal is first down-modulated before the information is extracted from the chaotic signal (Fig. 2).

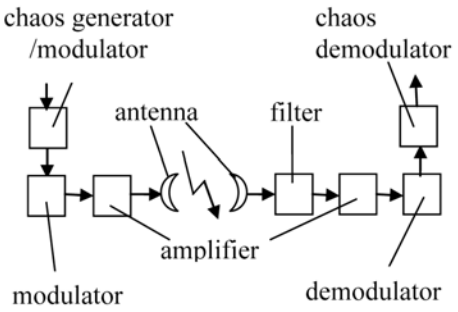

Fig. 2. Block diagram for CSK and DCSK

In principle, CSK and DCSK could also be applied for direct communications and therefore avoiding the implementation of power-consuming additional modulators and demodulators, but given the high frequencies involved, this is out of the reach of current technology. A prototype system on the basis of frequency modulated DCSK (FM-DCSK) has been built and successfully tested [14].

The advantages of using chaos for this class of methods are:

- Relatively simple implementation and thus potentially also a lower power consumption.
- Good robustness properties with respect to interferences

It must be admitted, though, that the second point has in general (beyond additive white gaussian channel noise) not been seriously addressed in the research literature, except for DCSK in [15]. The reason is that the performance for AWG noisy channels is not sufficiently good to motivate communication systems engineers to cross the threshold and invest in understanding techniques based on chaos. In fact, so far, to get close to the performance levels of the basic phase shift keying (PSK) or quadrature amplitude modulation (QAM) already is considered an achievement in the chaos communications community.

Help from information theory

We have wondered whether a better understanding of the situation could be provided by information theory. We were asking whether

- The mediocre performance of CSK, and to a minor extent also DCSK, could be understood by information theoretic arguments
- Whether chaotic signals by their very nature are a bad choice for good performance in communicating over AWGN channels.

Today, we believe that the answer to the first question is “yes” and to the second question “no”. This shall be explained in some more detail.

The principle of CSK is schematically represented in Figure 3.

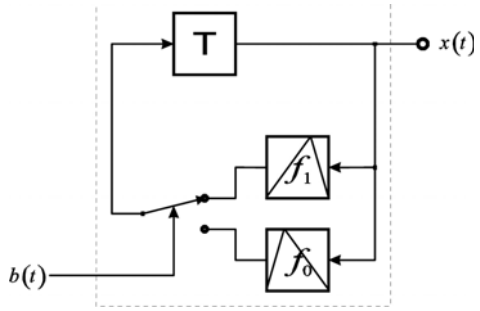

Fig. 3. Block diagram of a chaos shift keying (CSK) transmitter

Depending on the transmitted bit at time t (0 or 1), the transmitter sends a certain number of iterations of the function f_0 or f_1 over the noisy channel. This signal, corresponding to a single bit, is the time-discrete but value-continuous spreading sequence. Note that, unlike conventional DS-CDMA, not only the spreading sequence is not quantized, but it also never repeats. This can be considered an advantage, because the power spectrum of the sent signal has no peak at the frequency at which the bit is transmitted. However, it makes the decoding much more difficult.

At the receiver, it has to be decided, whether the noise-corrupted spreading sequence has been produced by f0 or f1. In the early days of CSK, this was done by chaos synchronization [7, 8, 9].

Unfortunately, straight-forward synchronization was too sensitive to noise perturbation in the channel, and more sophisticated demodulation/decoding methods had to be used [11]. Indeed, this improved the noise-efficiency of the method greatly, but not enough to motivate “communication engineers not already committed” to chaos-communications.

Paper [16] gives the answer. It reminds the readers the well known fact that the chaotic signal, due to its expansive nature that amplifies differences in initial conditions, intrinsically produces at each iteration information about the initial condition of the spreading sequence. In CSK, this unused information has to share the channel capacity with the information that interests us, the use of the functions f0 or f1 for each iteration. Therefore, in this context only two approaches can, in principle, get a noise efficiency close to Shannon’s limit, namely to code information on the initial conditions, or to prevent the information about the initial condition to transit on the channel. The second approach will be discussed in the next section.

In paper [11] a clear hint to the fact that chaotic signals can be used for channel coding is given and that nothing of fundamental nature prevents them from achieving Shannon’s limit for AWGN channels. In order to prove this conclusively, one would have to give an explicit block channel coding method, which in the limit of infinite codeword length reaches the performance of Shannon’s capacity, as is been done in the classical proof [17] using stochastic signals. Of course, such a channel coding method would be too complex to be used for any practical purpose, but it definitely would answer the second question posed above. In paper [11], actually decoding is done using only a simple threshold decision. It would be practical, but it does not achieve Shannon’s capacity. Nevertheless it is orders of magnitudes wrong which makes us believe that the answer to question 2 should be “no”.

Coded modulation using chaotic systems

We now return to the idea to code information onto the initial condition of the spreading code, or, more generally, on the initial conditions of the chaotic signal sent over the channel, not specifying at this point the method the modulation method.

There is a powerful mathematical theory for chaotic systems, or at least for a substantial subset of them: Symbolic analysis [18]. It associates with a chaotic trajectory, usually but not necessarily in discrete time, a binary signal. This correspondence is usually straight forward, just divide the state space into a two regions, label them with 0 and 1, and associate at each time with the state of the system the label of the region. This immediately gives a method to

code binary information onto a chaotic trajectory.

Just send the chaotic signal over the channel whose symbolic signal is the information to be transmitted. The problem with this procedure is that one would have to set the initial conditions of the trajectory with unrealistic precision. The way to avoid this is to control the trajectory with small control inputs. This method of communications using chaos has already been proposed a decade ago [19, 20]. Also, such small perturbation control has been found to be feasible for several "more physical" chaotic oscillators such as the Lorenz system [24].

As a result, we can code the payload information directly onto the symbolic sequence generated by the chaotic system (which is equivalent to assigning different initial conditions to different codewords). While in [11] we have demonstrated the feasibility of such an approach in principle, a constructive solution to the problem requires a careful choice of both the chaotic system (in particular the associated nonlinearity) as well as the set of initial conditions representing the codewords.

One possible class of chaotic systems for which the problem of both system design and codeword assignment can be solved in a relatively systematic way is the class of iterated piecewise linear Markov maps. Here, the notion of symbolic dynamics is particularly intuitive, as the symbols can be assigned directly to the intervals of the map and it can be shown that such assignment is "sufficient" in the sense that it covers the entire information production of the chaotic system in the sense of a Shannon and Kolmogorov-Sinai entropy.

With a control action given by $x(t+1)=f(x(t)) + b(t)\cdot q/2$ (for suitable maps $f(.)$ such as the Bernoulli shift map or the tent map, and for suitable coupling coefficients $q=2-Q$), there is in fact a discrete set of $2Q$ invariant points under this iteration, which allows to control the symbolic sequence [18] with a delay of Q iterations. It has been shown [21] that such a structure can be equivalently represented by a shift register structure with a mapping function generating the output $x(t)$ as a function of its state $b(t)\ldots b(t-Q)$. Such structure is known as a trellis coded modulation in communication theory [22], and the study of the performance of such systems is linked to the study of the embedded convolutional code.

In order to identify chaotic maps which optimize the performance of such schemes, the analysis of the system performance in terms of Minimum distance error events [22] can be carried out [21], illustrating close-to-BPSK performance for the Bernoulli shift map, while for the tent map, the performance is bad.

It turns out that performance can be improved beyond BPSK by combining the classical CSK approach shown in Figure 3 with the small perturbation control such that both inputs (the control sequence and the sequence switching the maps) is driven by the same (payload) data [21] and an appropriate choice of the maps f_0 and f_1. This principle is illustrated in Figure 4 below.

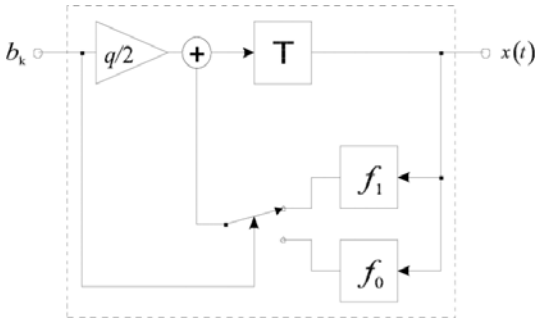

Fig. 4. Block diagram of a CSK transmitter with small perturbation controlled symbolic dynamics

This underlines again our answers to the questions 1 and 2 as given above, as for the given example they have both been addressed in a constructive way.

Conclusion

We have given a survey of approaches to communications with chaotic systems developed in the last 10 years. Given the generally mediocre performance of such approaches, we have identified two fundamental questions which should help us pinpoint the main problems with the existing approaches with the help of information theory and communication theory.

In particular it has been confirmed both in theory and by a constructive approach leading to a controlled variant of CSK, that indeed the information generated by free running chaotic systems (as captured by the Kolmogorov-Sinai entropy) is the problem, and the solution is a suitable control that makes this information part of the payload.

We believe that the approach demonstrated for the simple small perturbation controlled CSK transmitter is much more general and will find its application to "more physical" chaotic systems in the near future, leveraging the advantages of chaotic systems as given in the introduction.

Acknowledgments

This work has been financially supported the Swiss National Science Foundation, grant. 200021-100031. Slobodan Kozic and Kumiko Oshima are thanked for discussions on coded modulation.

References

[1] M. Delgado-Restituto, A. Rodriguez-Vazquez. Integrated chaos generators, *Proc. IEEE*, vol.90, no.5, pp. 747-767, 2002.

[2] A. Baranowski, W. Schwarz. Statistical analysis and design of continuous-discrete chaos generators, *Trans. IEICE*, Vol. E82-A, No. 9, pp. 1762-1768, 1999.

[3] R. Rovatti, G. Mazzini, G. Setti, A. Giovanardi. Statistical modeling and design of discrete-time chaotic processes: advanced finite-dimensional tools and applications, *Proc. IEEE*, Vol. 90, No. 5, pp. 820-841, 2002.

[4] A. Dmitriev, B. Kyarginsky, A. Panas, S. Starkov. Direct chaotic communication scheme at microwave frequencies, *J. of Communications Technology and Electronics*, v. 46, no. 2, pp. 207-214, 2001.

[5] R. Rovatti, G. Mazzini, G. Setti. Interference bounds for DS- CDMA systems based on chaotic piecewise affine Markov maps, *IEEE Trans. Circ. Syst. I*, vol.47, No.6, pp.885-896, 2000.

[6] R. Rovatti, G. Mazzini, G. Setti. Enhanced rake receivers for chaos-based DS-CDMA, *IEEE Trans. Circ. Syst. I*, vol.48, No. 7, pp. 818-829, 2001.

[7] H. Dedieu, M.P. Kennedy, M. Hasler. Chaos shift keying: modulation of a chaotic carrier using self-synchronizing Chua's circuits, *IEEE Trans. Circ. Syst. II*, Vol.40, pp. 634-642, 1993.

[8] Yu.L. Bel'skii, A.S. Dmitriev. Information transmission using deterministic chaos (in Russian), *Radiotechnika i Elektronika (Russian Academy of Science)*, Vol.38, pp. 1310-1315, 1993.

[9] C.W. Wu, L.O. Chua. Transmission of digital signals by chaotic synchronization, *Int. J. Bif. Chaos*, Vol.3, no.6, pp. 1619-1627, 1993.

[10] G. Kolumban, K. Vizvari, A. Abel, W. Schwarz. Differential chaos shift-keying: a robust coding for chaos communication, *Proc. NDES 1996*, Seville, Spain, pp. 87-92, 1996.

[11] M. Hasler, T. Schimming. Optimal and suboptimal chaos receivers, *Proc. IEEE*, vol.90, no.5, pp.733-746, 2002.

[12] A. Abel, W. Schwarz. Chaos communications – principles, schemes and system analysis, *Proc. IEEE*, vol.90, no.5, pp. 791-710, 2002.

[13] G. Kolumban, M.P. Kennedy, Z. Jako, G. Kis. Chaotic communications with correlation receivers: theory and performance limits, *Proc. IEEE*, vol.90, no.5, pp. 711-732, 2002.

[14] K. Krol, L. Azzinnari, E. Korpela, A. Mozsari, M. Talonen, V. Porra. An experimental FM-DCSK chaos radio system, *Proc. ECCTD-2001*, Espoo, Finland, vol.3, pp. 17-20, 2001.

[15] M.P. Kennedy, G. Kolumban, G. Kis, Z. Jako. Performance evaluation of FM-DCSK modulation in multipath environments, *IEEE Transaction on Circuits and Systems*-1, Vol. 47, pp. 1 772-1711, 2000.

[16] T. Schimming. Chaos based modulations from an information theory perspective, Proc. ISCAS 2001, Sidney, Australia, Vol.3, pp. 309-312. 2001.

[17] T. Cover, J. Thomas. *Elements of information theory*, Wiley & Sons, New York, 1991.

[18] Hao Bai-lin. *Applied symbolic dynamics and chaos*, World- Scientific, Singapore, 1998.

[19] S. Hayes, C. Grebogy, E. Ott. Communicating with chaos, Phys.Rev.Lett., Vol.70, pp. 3031-3034, 1993.

[20] J. Schweizer, M.P. Kennedy. Predictive Poincaré control modulation: a new method for modulating digital information onto a chaotic carrier signal, Irish DSP and Control Colloquium, Dublin, Ireland, pp.125-132. 1994.

[21] S. Kozic, K. Oshima, T. Schimming. Minimum Distance Properties of coded modulations based on iterated chaotic maps, Proc. ECCTD 2002, Krakov, Poland, 2003.

[22] J.G. Proakis, *Digital Communications*, McGraw-Hill, 1995.

INTERNATIONAL CONFERENCE "ENGINEERING MANAGEMENT OF COMMUNICATION AND TECHNOLOGY" (EMCTECH)

FINAL INFORMATION AND STATISTICS

Svetlana Dymkova, Oleg Varlamov
Institute of radio and information systems (IRIS), Vienna, Austria

DOI: 10.36724/2664-066X-2021-7-6-36-39

International conference "ENGINEERING MANAGEMENT OF COMMUNICATION AND TECHNOLOGY" (EMCTECH) was held on October 20-22, 2021 in Vienna (Austria).

On EMCTECH-2021 was invited researchers, educators, managers, and students, which research activity, case studies or best practices, shedding light on the theory or practice of engineering, technology, innovation management, or development of personal skills, business and entrepreneurship [1, 2, 7].

Conference organizers:

- Institute of Electrical and Electronics Engineers (IEEE);
- Institute of radio and information systems (IRIS), Vienna, Austria).

All accepted and presented Papers following the conference will be submitted for inclusion into IEEE Xplore and will be submitted also for indexing in Scopus and Web of Science data bases.

Field of interest on EMCTECH-2021:

- Technology advancements in IoT devices, artificial Intelligence, Broadcasting, wire and optical communication;
- New opportunities using technology in BioMedical, Farming, Transportation, and Cyber Physical Systems;
- Digital Transformation and Data Risk Management in ICT/Telecommunication, smart cities, public policy;
- Engineering technology leading to social, political and economical change.

On EMCTECH-2021 IEEE in cooperation with Institute of Radio and Information Systems (IRIS) provide various opportunities for publishing results of research, based on international scientific and technical cooperation of researchers, PhD students and students in the field of radio and information systems.

Reports presented at the conference in 6 sections:

- Technology advancements in IoT devices & artificial intelligence
- Transport and collective systems: smart control technology in transportation, biomedical, farming and cyber physical systems (new opportunities using technology in biomedical, farming, transportation, and cyber physical systems)
- Broadcast technologies advancements – radio, IP, cellular, on demand, interactive, wire and optical communication
- Information process management in digital society and industry 4.0
- Digital transformation and data risk management in ICT/telecommunication
- Engineering technology leading to social, political and economical change.

EMCTECH TOTAL STATISTICS (IEEE Conference Record # 53459)

Year	Applications	Accepted papers	% of accepted papers	IEEE Members - Conference Participants	Conference participants	Conference authors	Organizations	Cities	Countries/ Continents
2020	95	57	60	10	201	139	38	17	12/5
2021	46	28	60	10	80	65	31	25	22/5

Participants with reports from 25 cities took part in the conference: Almaty (Kazakhstan), Athens (Greece), Baku (Azerbaijan), Bishkek (Kyrgyzstan), Brazzaville (Congo), Brisbane (Australia), Bujumbura (Burundi), Gdansk (Poland), Geneva (Switzerland), Ha Noi (Vietnam) Hamilton (New Zealand), Ilmenau (Germany), Jyvaskyla (Finland), London (United Kingdom), Moscow (Russia), New Delhi (India), Penza (Russia), Prague (Czech Republic), Pulheim (Germany), Pune (Republic of India), Punjab (Pakistan), Salvador (Republic of Brasil), Shandong (China), Trento (Italy), Vienna (Austria).

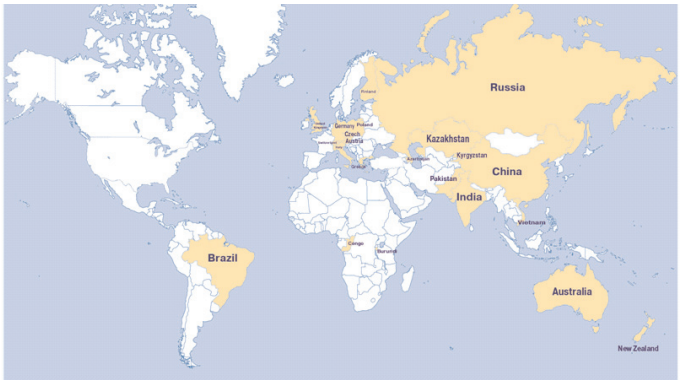

INVITED TALKS

Report by Dr. Julius Golovatchev, Anton Bezlakovskii, Evgeniy Bezlakovskii and Georg Kirchgessner, INCOTELOGY GmbH, Pulheim, Germany

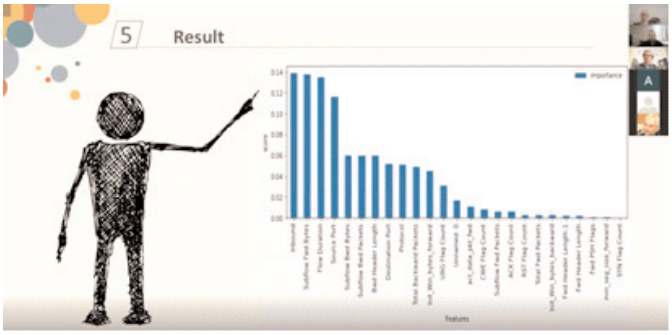

Report by Anshita Dhoot, Karan Singh, School of Computer & Systems Sciences, Jawaharlal Nehru University, New Delhi, India, Boyang Zong, Department of Computer Science & Technology, Qilu University of Technology, Shandong, China and Salman Saeed, Department of Information & Communication Engineering, Islamia University of Bahawalpur, Punjab, Pakistan

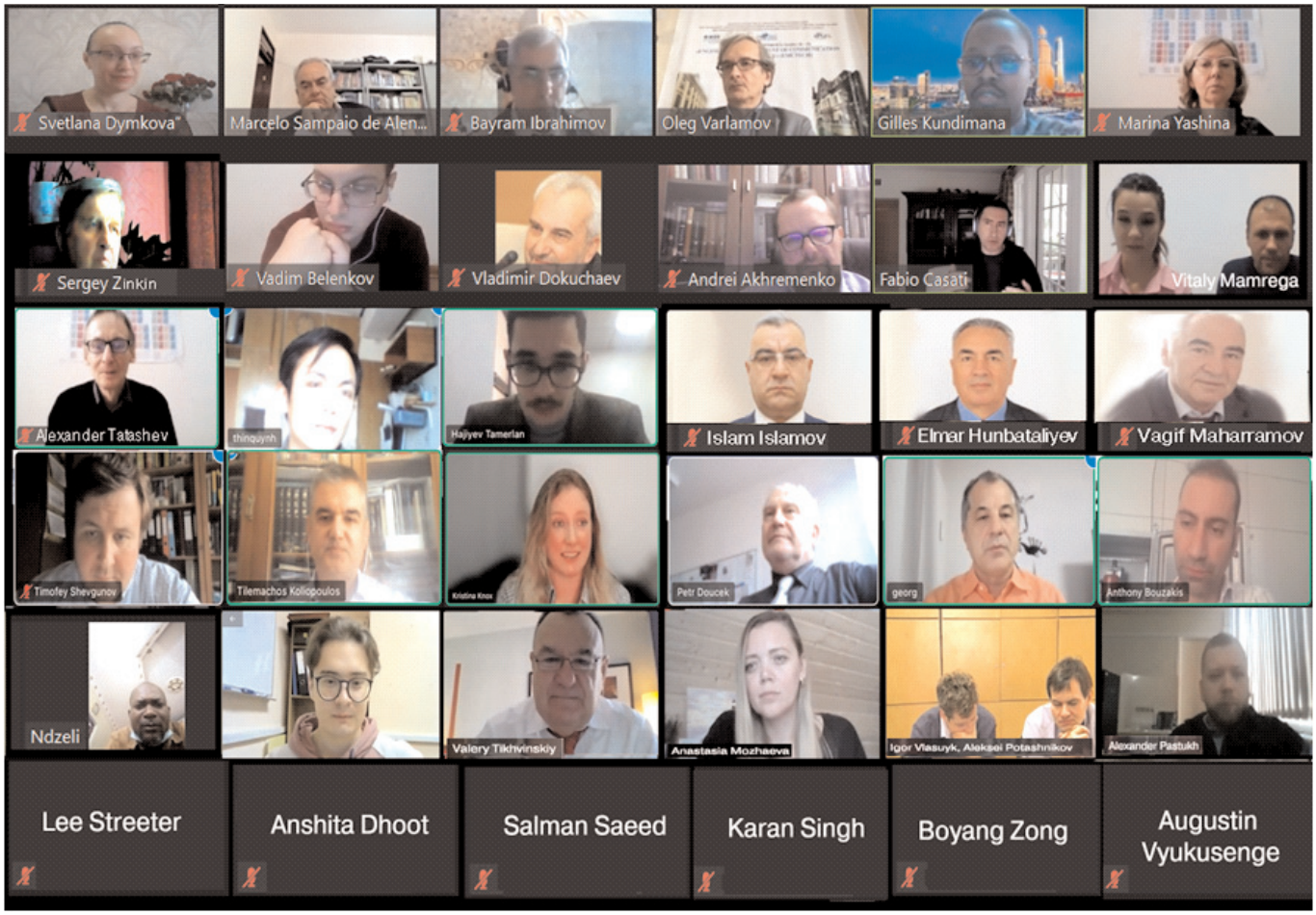

WEBINAR FOR UNDERGRADUATE AND GRADUATE STUDENTS
(Second conference day, 21 October 2021)

"FUNDAMENTALS OF SCIENTIFIC RESEARCH": AUTHOR'S PROFILES IN SCIENTOMETRIC DATABASES

SPEAKERS

Albert Waal, RFmondial GmbH, Hannover, Germany
Oleg Varlamov, Institute of Radio and Information Systems (IRIS Association), Vienna, Austria
Angelina Bott, City Administration, Bad Wildbad, Germany
Augustin Vyukusenge, University of Burundi, Bujumbura, Burundi
Svetlana Dymkova, Institute of Radio and Information Systems (IRIS Association), Vienna, Austria

Unique author identifiers in the information systems make it possible to establish an unambiguous correspondence between the author and his scientific publications, eliminating the problem of the plurality of spelling of the surname (namesakes, change of surnames, incomplete indication of names in publications, various transliterations etc.). It is possible to accurately measure citation rate of the works of individual researchers, to facilitate the process of assessing productivity and influence of both a particular author and a scientific organization by summing up the activities of its employees [3].

An author's profile is a collection of information in a scientometric database about the author's place of work, number of his publications and their citation rate, years of publication activity, research area, co-authors, Hirsch index, a list of literary sources used in works, etc. Each author's profile is assigned a unique identifier [6].

This webinar contains step-by-step instructions for creating author profiles in international author registration systems [8]. The manual was developed to improve the presentation of information about publications of students and university staff in citation indexes (Web of Science, Scopus), as well as in international author registration systems (ResearcherID, ORCID, Google Scholar, etc.).

Information about the authors' publications used for the purpose of calculating individual achievements upon admission to the magistracy and postgraduate studies, establishing additional payments, bonuses, when holding competitions for the replacement of positions, competitions for the provision of funds for participation in conferences, grants, etc., the administrative services of universities are obtained on the basis of information about the identifiers of the authors in the corresponding citation indices or author registration systems [4,5]. Publications that are not tied to the corresponding author profiles are not taken into account when analyzing the publication activity of the authors.

COURSE CONTENTS

LESSON 1.
CREATING AN AUTHOR'S PROFILE IN GOOGLE SCHOLAR AND MAINTAINING HIS PERSONAL PAGE IS AN IMPORTANT FACTOR IN THE AUTHOR'S REPRESENTATION IN INFORMATION ENVIRONMENT OF THE WORLD SCIENTIFIC COMMUNITY

Google Scholar is one of the most widely used full-text search engines for scientific publications of all formats and disciplines, as well as indexing by various indicators. At the moment, it is the world's most popular search engine for scientific publications, including articles, dissertations, books, abstracts and reports published by scientific literature publishers, professional associations, universities and other scientific organizations.

The fundamental difference between Google Scholar and similar systems (databases, citation indexes) is that the number of publications indexed and displayed in Google Scholar automatically (as a result of the work of search robots) includes those publications for which data (including metadata, PDFs with full text) are available on the Internet.

For an organization, the registration of its authors in Google Scholar is important for increasing the organization's representation in information environment of the world scientific community and for systematizing and structuring data on publications and citations of employees' publications available in Google Scholar. Further correct indexing according to these indicators is necessary for the correct accounting of these indicators and the promotion of organization in various webometric ratings.

LESSON 2.
ORCID ID REGISTRATION, MANAGEMENT OF THE RECORD RESULTS AND ACTIVITIES, SEARCH IN THE REGISTER OF OTHER SCIENTISTS

ORCID is an open, non-profit organization. ORCID's work is aimed at creating and maintaining a registry of unique identifiers for researchers and the link between research papers and their results and these identifiers. The ORCID project is unique in that it is not limited by the framework of a specific scientific discipline, research section and state boundaries. The ORCID registry allows researchers to link researchers to their performance by integrating the ORCID iD into key processes such as updating an investigator's dossier, reviewing manuscripts, and applying for grants and patents.

The ORCID accounting system provides two main features:

1. A registry where ou can get a unique identifier and manage the record of research results.
2. D elopment interfaces (API), designed to ensure the transfer of data between different accounting systems and the establishment of authorship of scientific papers in each of them. ORCID software is distributed under a free license. The free download database is updated every year and operates under a copyright waiver and public domain release tool.

Individual researchers can obtain an ORCID ID, manage their records, and search the registry for other researchers. Research organizations can become participants in the ORCID project to link ORCID IDs to records stored in local databases, to update records in the registry and receive notifications about ORCID work, as well as to register their employees and students and receive an ORCID ID.

LESSON 3.
REGISTRATION AND WORK IN RESEARCHGATE

ResearchGate is a free social network and collaboration tool for scientists from all scientific disciplines. It provides web-based applications such as semantic search (search by annotation), file sharing, sharing a publication base, forums, methodological discussions, and so on.

One of the distinguishing features of ResearchGate is its semantic search engine, which indexes both internal resources and the main public article databases, including PubMed, CiteSeer, arXiv, NASA Library.

This search engine was specially designed to analyze entire

article abstracts (not just keywords), which should improve the accuracy of the results. A similar semantic match search engine is used to offer new social connections to network participants. After analyzing the information specified by the user in his profile, the site offers close to the interests of the user of the group, other members and literature. In total, more than 1,100 groups have been created. Groups can be both open and closed. Any user can always create a new group.

The group offers collaboration support tools such as file sharing tools. There are also tools for scheduling meetings and organizing surveys. Several academic organizations and conferences use ResearchGate as their primary means of communicating with participants. The site also offers the possibility of creating subgroups for large organizations, open only to members from the respective institution.

ResearchGate makes it possible to download recently published articles while respecting copyright. These articles are automatically indexed by the site's search engine. Users can read and download articles for free.

LESSON 4.
WORKING WITH AN AUTHOR PROFILE IN SCOPUS

Scopus is a bibliographic and abstract database and citation tracking tool for articles published in scientific journals. The database indexes scientific journals, conference proceedings and serial books, as well as Trade Journals. Scopus is developed and owned by Elsevier Publishing Corporation. The database is available on a subscription basis via the web interface. The search engine is integrated with the Scirus web search engine and patent database. For authors who have published more than one article, individual accounts are created in Scopus - author profiles with unique author identifiers (Author ID).

These profiles provide information such as variations of the author's name, list of places of work, number of publications, years of publication activity, research areas, links to main contributors, total number of citations per author's publications, total number of sources cited by the author, Hirsch index of the author etc.

The database provides users with the ability to use unique author identifiers to generate search queries and set up email or RSS alerts for changes in author profiles. The possibilities of searching for authors and limited viewing of their profiles are available without a subscription to the Scopus database using the Scopus Author Preview.

Similar to author profiles, for institutions whose employees have published more than one article, Scopus creates profiles with unique identifiers of institutions (Scopus Affiliation Identifiers). These profiles provide information such as the address of the institution, the number of staff authors of the institution, the number of staff publications, a list of the main titles of the publications in which the staff of the institution are published, and a chart of thematic distribution of publications of the staff of the institution.

LESSON 5.
CREATING AND WORKING WITH AN AUTHOR PROFILE IN WEB OF SCIENCE

Web of Science (WoS) is a multidisciplinary platform that helps you quickly find, analyze and share information in the natural sciences, social sciences, humanities, and arts. The user has integrated access to high-quality literature through a unified platform that links a wide variety of content and search terms together to create one common vocabulary and one comprehensive search. Developed by Thomson Reuters, currently owned by Clarivate Analytics, and available by subscription. The platform has built-in capabilities for searching, analyzing and managing bibliographic information. The core of the platform is the Web of Science Core Collection database.

ResearcherID (currently the service has been expanded and renamed Publons, and the ResearcherID name remains only as an author's identifier) is a free resource for the worldwide polythematic scientific community. After registration, the user is assigned an individual identification number, which is retained for the entire time of work, regardless of the change in the name or affiliation of the organization.

Publons allows you to create a profile online to present your publication history. The resource is designed to connect the user with his scientific work, which provides an accurate record of the output and authorship. It also enables colleagues to quickly locate a user's published work and identify him as a potential collaborator. Publons tools include an interactive lab environment for exploration of author-level metrics. These tools allow you to perform visual analysis of research networks in accordance with the following parameters: subject category; country / territory; organization; author's name; year of publication; geographical position.

Media partner of EMCTECH-2021 – an open access journal by MDPI – Sensors.

References

[1]. O. Varlamov, S. Dymkova, "Preface of the 2020 international conference on engineering management of communication and technology (EMCTECH)," *2020 International Conference on Engineering Management of Communication and Technology (EMCTECH)*, 2020, 10.1109/EMCTECH49634.2020.9261523.

[2]. O. V. Varlamov, S. Dymkova, "Preface of the 2021 International Conference on Engineering Management of Communication and Technology (EMCTECH)," *2021 International Conference on Engineering Management of Communication and Technology (EMCTECH)*, 2021, pp. 1-7, doi: 10.1109/EMCTECH53459.2021.9619175.

[3]. R. R. Fayzullin, I. M. Lerner, N. M. Solodukho, S. S. Dymkova and V. I. Il'in, "Formation of a Competency Model in Teaching Students of Technical Universities with Hearing Impairment, which Implements a Conveyor-Based Approach to Learning," *2021 Systems of Signal Synchronization, Generating and Processing in Telecommunications (SYNCHROINFO*, 2021, pp. 1-4, doi: 10.1109/SYNCHROINFO51390.2021.9488367.

[4]. S. S. Dymkova, "Breakthrough 5G data call using dynamic spectrum sharing to accelerate nationwide 5G deployments," *Synchroinfo Journal*, vol. 5, no. 6, pp. 17-21, 2019.

[5]. S. Dymkova, "Applicability of 5G subscriber equipment and global navigation satellite systems," *Synchroinfo Journal*, vol. 7, no. 5, pp. 36-48, 2021. DOI: 10.36724/2664-066X-2021-7-5-36-48.

[6]. S. S. Dymkova, "Development of information system for promotion of scientific research results", *T-Comm*, vol. 11, no. 7, pp. 38-41, 2017.

[7]. S. S. Dymkova, "Identifying and Implementing Successful Scientific Projects in the Framework of "IEEE Technology and Engineering Management Society Events", *2020 International Conference on Engineering Management of Communication and Technology (EMCTECH)*, pp. 1-7, 2020.

[8]. Varlamov O. V., Dymkova S. S., Gorodilina M. V. Author's profiles in scientometric databases. Moscow, 2020.

INTERNATIONAL CONFERENCE

«2022 International Conference «Engineering Management of Communication and Technology» (EMCTECH)

IEEE Conference

20 – 22 October 2022
Vienna, Austria

Conference will produce a publication.

All accepted and presented Papers following the conference will be submitted for inclusion into IEEE Xplore and will be submitted also for indexing in Scopus and Web of Science data bases

The papers which are discussed at the conference can be divided into the following chapters:

CHAPTER 1. TECHNOLOGY ADVANCEMENTS IN IOT DEVICES

CHAPTER 2. TECHNOLOGY ADVANCEMENTS IN ARTIFICIAL INTELLIGENCE
Subsection 2.1. Philosophy of Artificial Intelligence – Man in Intelligent Communication Systems

CHAPTER 3. TRANSPORT AND ?OLLECTIVE SYSTEMS: SMART CONTROL TECHNOLOGY IN TRANSPORTATION, BIOMEDICAL, FARMING AND CYBER PHYSICAL SYSTEMS (new opportunities using technology in biomedical, farming, transportation, and cyber physical systems)
Subsection 3.1. Technology advancements in creating sustainable engines
Subsection 3.2. Smart Highway Maintenance: Advanced Technology of Control and Design

CHAPTER 4. BROADCAST TECHNOLOGIES ADVANCEMENTS – RADIO, IP, CELLULAR, ON DEMAND, INTERACTIVE

CHAPTER 5. TECHNOLOGY ADVANCEMENTS IN WIRE AND OPTICAL COMMUNICATION AND CONTROL SYSTEMS

CHAPTER 6. DIGITALIZATION PROCESS AND SECURITY MANAGEMENT IN DIGITAL SOCIETY AND INDUSTRY 4.0

CHAPTER 7. DIGITAL TRANSFORMATION AND DATA RISK MANAGEMENT IN ICT/TELECOMMUNICATION

CHAPTER 8. DEVELOPING PERSONAL SKILLS FOR LEADING INNOVATION INITIATIVES

CHAPTER 9. ENGINEERING TECHNOLOGY LEADING TO SOCIAL, POLITICAL AND ECONOMICAL CHANGE

Submission dates

Full Paper Submission date: 15 August 2022

Notification of Acceptance date: 30 August 2022

Materials are available in English

http://media-publisher.eu/conference-emctech/call-for-papers/